$\mathbb{Z}_N$ lattice gauge theories with matter fields

Kaustubh Roy [1,2] and Elio J. König [2]
[1]*Indian Institute of Science, CV Raman Road, Bengaluru 560012, India*
[2]*Max-Planck-Institut für Festkörperforschung, Heisenbergstraße 1, 70569 Stuttgart, Germany*

(Received 17 September 2023; revised 22 March 2024; accepted 28 March 2024; published 1 May 2024)

Motivated by the exotic phenomenology of certain quantum materials and recent advances in programmable quantum emulators, we here study fermions and bosons in $\mathbb{Z}_N$ lattice gauge theories. We introduce a family of exactly soluble models, and characterize their orthogonal (semi)metallic ground states, the excitation spectrum, and the correlation functions. We further study integrability-breaking perturbations using an appropriately derived set of Feynman diagrammatic rules and borrowing physics associated to Anderson's orthogonality catastrophe. In the context of the ground states, we revisit Luttinger's theorem following Oshikawa's flux insertion argument and furthermore demonstrate the existence of a Luttinger surface of zeros in the fermionic Green's function. Upon inclusion of perturbations, we address the transition from the orthogonal metal to the normal state by condensation of certain excitations in the gauge sectors, so-called "*e* particles." We furthermore discuss the effect of dynamics in the dual "*m*-particle" excitations, which ultimately leads to the formation of charge-neutral hadronic *N*-particle bound states. We present analytical arguments for the most important phases and estimates for phase boundaries of the model. Specifically, and in sharp distinction to quasi-one-dimensional $\mathbb{Z}_N$ lattice gauge theories, renormalization group arguments imply that the phase diagram does not include an emergent deconfining U(1) phase in the limit of large number of fermion flavors. Therefore, in regards to lattice QED problems, $\mathbb{Z}_N$ quantum emulators with $N < \infty$ can at best be used for approximate solutions at intermediate length scales.

DOI: 10.1103/PhysRevB.109.195108

I. INTRODUCTION

Lattice gauge theories (LGTs) have enjoyed constant interest throughout the decades. Originally introduced in the context of statistical physics [1], they have since been of extraordinary relevance to understanding the strong coupling limit of the standard model of elementary particles [2–4] and to exotic phases of quantum materials [5], including quantum spin liquids [6]. While theoretical activity is motivated by the fundamental connection of gauge theories to states with topological order [7] and to topological quantum computing [8], very recent interest [9–14] was boosted by the (prospect of the) realization of lattice gauge theories in quantum emulators [15,16], in particular in the context of Rydberg atoms [17–20] and arrays of superconducting qubits [21–23], including proposed implementations of discrete $\mathbb{Z}_N$ gauge theories with $N > 2$.

From the perspective of quantum field theory, $\mathbb{Z}_N$ gauge theories coupled to fermionic matter are of considerable interest as toy models of hadron formation: for example, a finite string tension in $\mathbb{Z}_3$ gauge theories is expected [24] to favor baryonic gauge neutral fermionic trions, while in $\mathbb{Z}_2$ gauge theories mesonlike (Cooper) pairs are formed [25]. While even the physics of non-Abelian gauge theories may dynamically emerge [26], it is of interest to consider discrete $\mathbb{Z}_N$ LGTs with $N \gg 1$ as a proxy of U(1) LGT [27], which in contrast to quantum electrodynamics (QED) benefit from a finite local Hilbert space dimension which is more suitable to both classical numerical simulations and analog quantum emulations.

From the statistical mechanics viewpoint, pure $\mathbb{Z}_N$ lattice gauge theories in $D = 2 + 1$ are obtained from $\mathbb{Z}_N$ quantum clock models by Kramers-Wannier duality transformation [1,28]. This is in contrast to the case of $D = 1 + 1$ spacetime dimensions, in which the quantum clock model maps back onto itself. The differences between $D = 1 + 1$ and $D = 2 + 1$ persist to the nature of the (quantum) phase transition between ordered and disordered phases: While for quantum clock models for $N > 4$ and in $D = 1 + 1$, as well as for certain non-Hermitian perturbations of clock models in $D = 2 + 1$ [29,30] the direct quantum phase transition is replaced by two Berezinskii-Kosterlitz-Thouless–type phase transitions enclosing an intermediary gapless U(1) phase [31], for the quantum clock model in $D = 2 + 1$, the quantum phase transition is direct, yet of U(1) type [32,33]. What, however, if the $\mathbb{Z}_N$ gauge theory in $D = 2 + 1$ is coupled to fermionic matter fields [34–39]? Is an intermediate U(1) phase emerging in the same way as in ladder systems [40–42], where $\mathbb{Z}_N$-symmetry-breaking perturbations can be renormalization group (RG) irrelevant? An affirmative answer would clearly facilitate numerical studies of QED_3.

Finally, from the perspective of quantum materials, $\mathbb{Z}_N$ gauge theories with $N > 2$ have been very recently proposed to explain strange and bad metal behavior [43]. Quantum spin-liquid states with $\mathbb{Z}_N$ gauge group have also been studied over the years [44–46]. In general, fractionalization approaches to correlated systems, including slave rotors [47] which are related to the $N \to \infty$ limit of our theory, have been successfully employed (see, e.g., [48–52]). Of relevance for this work are studies of $\mathbb{Z}_2$ fractionalized metals [53–55] and of orthogonal (semi)metals in two spatial dimensions [25,26,56–58]. These states of matter can appear in $\mathbb{Z}_2$ slave spin constructions [59] and display a gap in the fermionic Green's function, as if they were an insulator, but sustain gapless two-body correlators, as if they were a metal. Fascinatingly, the deconfining phases of $\mathbb{Z}_2$ LGTs allow to circumvent [60–63] the Luttinger-Oshikawa theorem [64,65], i.e., the paradigm that in the absence of symmetry breaking the volume of the Fermi sea is determined by the fermion density alone, independently of the strength of interactions. Experimentally, this paradigm is challenged by the Fermi-surface reconstruction in the cuprates including the putative direct transition into the normal Fermi-liquid phase as observed in magnetotransport [66]. A similar scenario of Fermi-surface reconstruction in heavy-fermion materials [67] is corroborated by quantum oscillation experiments. Another remarkable conundrum is the observation of quantum oscillations in electrical insulators, most notably $YbAl_{12}$ [68] but potentially also in SmB_6 [69,70] and $RuCl_3$ [71], which suggest the presence of a "hidden" Fermi surface. More precisely than noted above, Luttinger's theorem identifies the density to the volume where the fermionic Green's function is positive, which is enclosed by the area of poles *or zeros* of the Green's function. Therefore, in addition to deconfining gauge theories, Luttinger's theorem may also be nontrivially satisfied in systems which stabilize a Luttinger surface of Green's function zeros [72]. This avenue, which has attracted substantial renewed attention recently [73–76], provokes the question if and when the LGT scenario and the scenario of Luttinger surfaces are two distinct descriptions of the same state of matter.

Here we study the $\mathbb{Z}_N$ toric code [8,77–82] coupled to fermionic matter, which realizes a $\mathbb{Z}_N$ LGT in $D = 2 + 1$ space-time dimensions including both bosonic and fermionic matter fields. We argue that such a model may describe strongly coupled quantum materials in which a slave-clock fractionalization scheme is accurate and summarize the duality mapping between our model and $\mathbb{Z}_N$ LGTs with both fermionic and bosonic matter fields. On the side, we mention that the interplay of fermions with toric code degrees of freedom resembles processes such as quasiparticle poisoning that can cause decoherence in topological quantum computing paradigms. Starting from the integrable limit describing the deconfining $\mathbb{Z}_N$ orthogonal (semi)metallic [56,83] phases we revisit Luttinger's theorem for arbitrary N and the question of Fermi-surface reconstruction without symmetry breaking. Upon inclusion of small perturbations, we demonstrate that $\mathbb{Z}_N$ orthogonal metals feature a Luttinger surface of Green's function zeros. We furthermore develop a diagrammatic perturbation theory allowing to resum perturbations and to determine the phases [84] of the $\mathbb{Z}_N$ LGT, their observable signatures, and the most important phase boundaries. We also present renormalization group calculations which imply that a putative deconfining intermediate phase of a U(1) LGT with a Fermi surface is unstable towards $\mathbb{Z}_N$ perturbations and thus absent in the phase diagram. Instead, we find the formation of hadrons (charge-neutral N-particle states) near the transition. It is to be noted that both the instability of hadron formation and the ruling out of a putative U(1) phase have been examined in the limit of large number of fermion flavors.

The remainder of the paper is structured as follows: In Sec. II we introduce the model in its integrable limit and motivate a $\mathbb{Z}_N$ fractionalization scheme. In Sec. III we find the ground state and excitations in the soluble limit. Section IV lays the modification to Luttinger's theorem obeyed by this ground state. In Sec. V, we develop Feynman rules and diagrammatics for the model. This allows perturbative addition of terms that destabilize the ground state and give rise to new phases, which are investigated in Sec. VI. In Sec. VII, we present renormalization group arguments for the absence of a U(1) phase. We conclude with a summary and outlook and delegate important technical details to the Appendixes.

II. MODEL AND MOTIVATION

In this section, the integrable limit of the model is introduced and motivated by a $\mathbb{Z}_3$ fractionalization of generalized Hubbard models. Integrability-breaking perturbations are discussed later, in Sec. VI.

A. Integrable limit

In its integrable limit, the model under consideration is described by a generalization of Kitaev's toric code with mobile fermions on the lattice, $\mathcal{H} = \mathcal{H}_K + \mathcal{H}_h + \mathcal{H}_w$, with

$$\mathcal{H}_K = -\frac{K}{2}\sum_{\mathbf{p}} e^{-i\phi} B_{\mathbf{p}} + \text{H.c.}, \tag{1a}$$

$$\mathcal{H}_h = -\frac{h}{2}\sum_{\mathbf{r}} e^{-i\theta} Q_{\mathbf{r}} + \text{H.c.}, \tag{1b}$$

$$\mathcal{H}_w = -w\sum_{\mathbf{r}}\sum_{\mathbf{e}\in\{\hat{x},\hat{y}\}} c^\dagger_{r,\alpha}\sigma_{\mathbf{r}+\frac{1}{2}\mathbf{e}} c_{r+\mathbf{e},\alpha} + \text{H.c.} - \mu\sum_{\mathbf{r}} c^\dagger_{\mathbf{r},\alpha} c_{\mathbf{r},\alpha}. \tag{1c}$$

Here and in what follows, $\mathbf{r}$, $\mathbf{b}$, and $\mathbf{p}$ denote the positions of vertices, bonds (or edges), and plaquettes (or faces) of the square lattice, and $c_{\mathbf{r}}$ are the fermionic annihilation operators in position space. In our notation, K, h, and w are real positive quantities and θ, ϕ are real angles. The quantities $B_{\mathbf{p}}$ and $Q_{\mathbf{r}}$ are the plaquette ("flux") and star ("charge") operators defined on the lattice as (see Fig. 1):

$$B_{\mathbf{p}} = \prod_{\mathbf{e}\in\{\hat{x},-\hat{y}\}} \sigma_{\mathbf{p}+\frac{1}{2}\mathbf{e}}\sigma^\dagger_{\mathbf{p}-\frac{1}{2}\mathbf{e}}, \tag{2a}$$

$$Q_{\mathbf{r}} = \omega^{\hat{\mathbf{n}}_{\mathbf{r}}} \prod_{\mathbf{e}\in\{\hat{x},\hat{y}\}} \tau_{\mathbf{r}+\frac{1}{2}\mathbf{e}}\tau^\dagger_{\mathbf{r}-\frac{1}{2}\mathbf{e}}. \tag{2b}$$

Here, $\hat{n}_{\mathbf{r}} = c^\dagger_{\mathbf{r},\alpha} c_{\mathbf{r},\alpha}$ is the fermionic density. The operators $\sigma_{\mathbf{b}}$, $\tau_{\mathbf{b}'}$ represent the $\mathbb{Z}_N$ clock variables at the bonds, satisfying the algebra

$$\sigma_{\mathbf{b}}\tau_{\mathbf{b}'} = (\omega)^{\delta_{\mathbf{b},\mathbf{b}'}}\tau_{\mathbf{b}'}\sigma_{\mathbf{b}}, \tag{3}$$

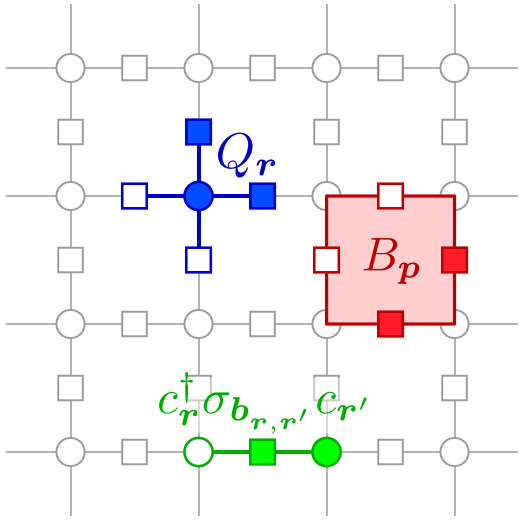

FIG. 1. The $\mathbb{Z}_N$ toric code, with the star, plaquette, and fermionic terms.

where $\omega \equiv \exp(\frac{2\pi i}{N})$ is the Nth root of unity. Fermions may or may not have an internal quantum number, e.g., a spin or flavor, $\alpha = 1, \ldots, N_f$ (where Einstein summation is implied throughout the paper).

One may use a series of well-known steps of gauge fixing to demonstrate that Eq. (1) is a $\mathbb{Z}_N$ gauge theory containing both fermionic and bosonic matter fields (see Appendix A for details). In the limit $h \to \infty, \theta = 0$, this model becomes a theory containing only gauge fields and fermions, complemented with a local Gauss' law $Q_{\mathbf{r}} = 1$ (no background $\mathbb{Z}_N$ charge).

B. Motivation: $\mathbb{Z}_3$ fractionalization of the Hubbard model

To heuristically motivate the $\mathbb{Z}_N$ gauge theory with fermions beyond the literature covered in the Introduction, we here review the basic aspects of a $\mathbb{Z}_3$ slave-spin fractionalization of a Hubbard-type single-band model

$$\mathcal{H} = -t \sum_{\langle \mathbf{r},\mathbf{r}' \rangle} c^\dagger_{\mathbf{r},\alpha} c_{\mathbf{r}',\alpha} + \sum_{\mathbf{r}} \frac{U}{2} n_{\mathbf{r}}(n_{\mathbf{r}} - 1) - \mu n_{\mathbf{r}} + \cdots . \quad (4)$$

The ellipsis denotes unknown additional terms which stabilize the fractionalized phase.

The local Coulomb repulsion splits the onsite energy into three distinct levels, with energies 0, μ, and $U - 2\mu$ and filling $n = 0,\ 1$, and 2, respectively. The $\mathbb{Z}_3$ slave spins act in the space of these three different charge states. This is similar to the well-established $\mathbb{Z}_2$ slave-spin approach [59], which, however, is applicable only to the special case $\mu = U/2$ in which the two levels with even fermion parity become degenerate. Generalizing the established approach leads to a $\mathbb{Z}_3$ fractionalization of the physical fermion operator [56]

$$c^\dagger_{\mathbf{r},\beta} = f^\dagger_{\mathbf{r},\beta} \varsigma_{\mathbf{r}}. \quad (5)$$

The f_β carries the fermion charge and spin, while the ς operator acts like a raising operator on the fermion occupancy basis $|n = 0, 1, 2\rangle$. The fractionalization has an emergent $\mathbb{Z}_3$ local symmetry $f_{\mathbf{r},\beta} \to e^{i\alpha_{\mathbf{r}}} f_{\mathbf{r},\beta}$, $\varsigma_{\mathbf{r}} \to e^{i\alpha_{\mathbf{r}}} \varsigma_{\mathbf{r}}$ with $\alpha_{\mathbf{r}} \in \{0, 2\pi/3, -2\pi/3\}$. It is generated by the unitary operator $Q_{\mathbf{r}} \equiv \omega^{-\hat{n}_{\mathbf{r}}} \boldsymbol{\tau}_r$, where $\omega \equiv e^{\frac{2\pi i}{3}}$ is the third root of unity and

$$\varsigma_{\mathbf{r}} = \begin{pmatrix} 0 & 1 & 0 \\ 0 & 0 & 1 \\ 1 & 0 & 0 \end{pmatrix}, \quad \boldsymbol{\tau}_{\mathbf{r}} = \begin{pmatrix} 1 & 0 & 0 \\ 0 & \omega & 0 \\ 0 & 0 & \omega^2 \end{pmatrix}. \quad (6)$$

The ς, $\boldsymbol{\tau}$ matrices suffice the same clock algebra [Eq. (3)] as σ, τ. In the process of fractionalization, we have artificially enlarged the Hilbert space. To return to the physical subspace, we impose the constraint

$$Q_{\mathbf{r}} = 1. \quad (7)$$

In this gauge sector, and up to a constant, the Hamiltonian takes the form

$$\mathcal{H} = -t \sum_{\langle \mathbf{r},\mathbf{r}' \rangle} f^\dagger_{\mathbf{r},\alpha} \varsigma_{\mathbf{r}} \varsigma^\dagger_{\mathbf{r}'} f_{\mathbf{r}',\alpha} - \frac{h}{2} \sum_{\mathbf{r}} (e^{-i\theta} \boldsymbol{\tau}_{\mathbf{r}} + \text{H.c.}) + \cdots , \quad (8)$$

where $he^{-i\theta} = [U - 3\mu - i\sqrt{3}(U - \mu)]/3$. Thus, for empty sites ($\mu \leqslant 0$), $\theta \in [-\pi/3, \pi/3]$, for single occupation ($0 \leqslant \mu \leqslant U$), $\theta \in [\pi/3, \pi]$ and for double occupation ($\mu > U$), $\theta \in [\pi, 5\pi/3]$.

At this point, the hopping term became an interaction term. Upon integration of high-energy modes in a renormalization group procedure, new operators may emerge. These include hopping of fermions

$$\mathcal{H}_w = -\frac{w}{2} \sum_{\mathbf{r},\mathbf{e}\in\{\hat{x},\hat{y}\}} \bar{\sigma}_{(\mathbf{r}+\frac{1}{2}\mathbf{e})} f^\dagger_{\mathbf{r},\alpha} f_{\mathbf{r}+\mathbf{e},\alpha} + \text{H.c.} \quad (9)$$

and bosons (clock degrees of freedom)

$$\mathcal{H}_J = -\frac{J}{2} \sum_{\mathbf{r},\mathbf{e}\in\{\hat{x},\hat{y}\}} \bar{\sigma}_{(\mathbf{r}+\frac{1}{2}\mathbf{e})} \varsigma^\dagger_{\mathbf{r}} \varsigma_{\mathbf{r}+\mathbf{e}}. \quad (10)$$

Note that by gauge symmetry, the new coupling constants obtained by contraction of the type $t\langle \varsigma_{\mathbf{r}} \varsigma^\dagger_{\mathbf{r}'} \rangle_{\text{fast}} = w\bar{\sigma}_{\mathbf{b}_{\mathbf{r},\mathbf{r}'}}/2$ retain a nontrivial transformation under gauge symmetry. To account for this, we introduce the emergent link degree of freedom (gauge potential) with nontrivial transformation $\bar{\sigma}_{\mathbf{b}_{\mathbf{r},\mathbf{r}'}} \to e^{i\alpha_{\mathbf{r}}} \bar{\sigma}_{\mathbf{b}_{\mathbf{r},\mathbf{r}'}} e^{-i\alpha_{\mathbf{r}'}}$ under $\mathbb{Z}_3$ gauge symmetry. In subsequent RG steps, terms accounting for the dynamics of gauge field variables emerge $\bar{\sigma}_{\mathbf{b}}$ (both electric and magnetic terms).

In Appendix A we provide details on the mapping [1,63,85] of the $\mathbb{Z}_N$ gauge theory of $f_{\mathbf{r}}, \varsigma_{\mathbf{r}}, \bar{\sigma}_{\mathbf{b}}$ variables to Eq. (1) with additional perturbations. In particular, the Gauss law as well as appropriate gauge fixing allows to remove $\varsigma_{\mathbf{r}}$ degrees of freedom from the Hamiltonian (1), which thereby takes the form of a toric code with integrability-breaking extra terms. Depending on the unspecified terms in the model indicated by the ellipsis, an effective low-energy deconfining state may be stabilized. While the nature of such stabilizing unknown terms is beyond the scope of the analysis in this paper, the present goal is to understand the physics of all such models which lie in the basin of attraction of the deconfining phase, i.e., of the ground state of Hamiltonian (1) discussed in the next section.

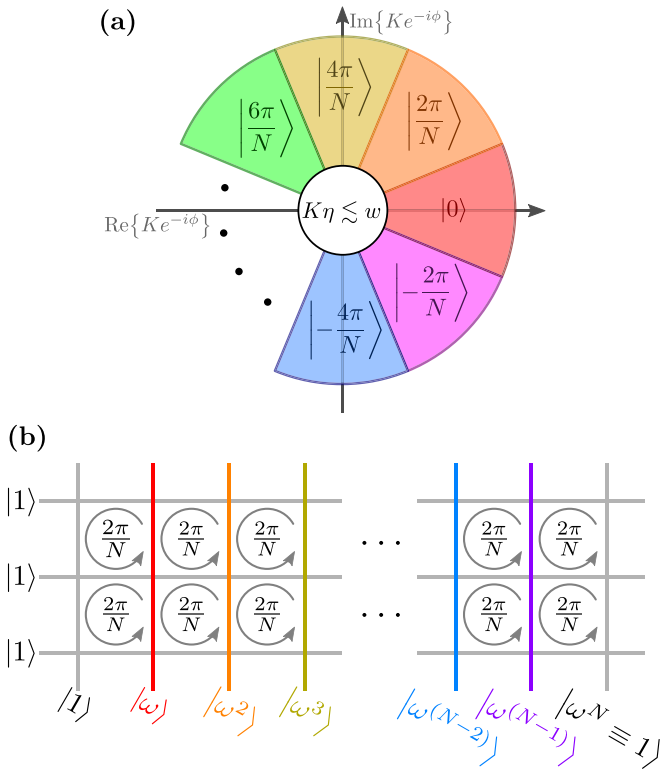

FIG. 2. (a) Phase diagram illustrating the ground state of the system $|\varphi\rangle$ as a function of the phase of $Ke^{-i\phi}$. A similar phase diagram occurs in the complex plane of $he^{-i\vartheta}$. (b) Landau gauge choice for the system with $2\pi/N$ flux. The entry inside kets indicates the eigenvalue of clock operators, $\sigma_{\mathbf{b}}|\omega^n\rangle = \omega^n|\omega^n\rangle$, on the corresponding links.

III. GROUND STATES AND EXCITATIONS

In this section, we determine the ground state of the model and the leading excitations in the model. As in the usual toric code, the plaquette and star operators mutually commute ensuring the integrability of the model. Moreover, they also commute with the fermionic term $\mathcal{H}_w$.

A. Ground state

In this paper, we will work in the asymptotic limit where the energy contribution of the fermionic part is negligible. We provide a mathematically concrete version of this qualitative statement at the end of the subsequent section (Sec. III B).

Since they commute with the Hamiltonian, each $B_{\mathbf{p}}$, $Q_{\mathbf{r}}$ individually encodes an integral of motion, with eigenvalues $1, \omega, \omega^2, ..., \omega^{N-1}$. The ground state has equal flux through all plaquettes $B_{\mathbf{p}}|\mathrm{GS}\rangle = e^{i\varphi}|\mathrm{GS}\rangle$ with $\varphi = \frac{2\pi n}{N}$ and equal charge on all sites $Q_{\mathbf{r}}|\mathrm{GS}\rangle = e^{i\vartheta}|\mathrm{GS}\rangle$ with $\vartheta = \frac{2\pi n'}{N}$ and $n, n' \in \{0, 1, \ldots, N-1\}$. The exact ground-state flux/charge is determined by minimizing the phase differences $\phi - \varphi$, $\theta - \vartheta$ [on the unit circle, see Fig. 2(a)].

To construct the ground state, we first set $h = 0$. We then choose a gauge configuration that satisfies the plaquette terms. For our analysis the "Landau" gauge is utilized [Fig. 2(b)], which corresponds to a wave function $|\varphi\rangle_\sigma = |\sigma_{\mathbf{b},\mathrm{horizontal}} = 1, \sigma_{\mathbf{b},\mathrm{vertical}} = \omega^{nb_x}\rangle$. To satisfy the Hamiltonian for $h > 0$, we project the constructed state onto the subspace

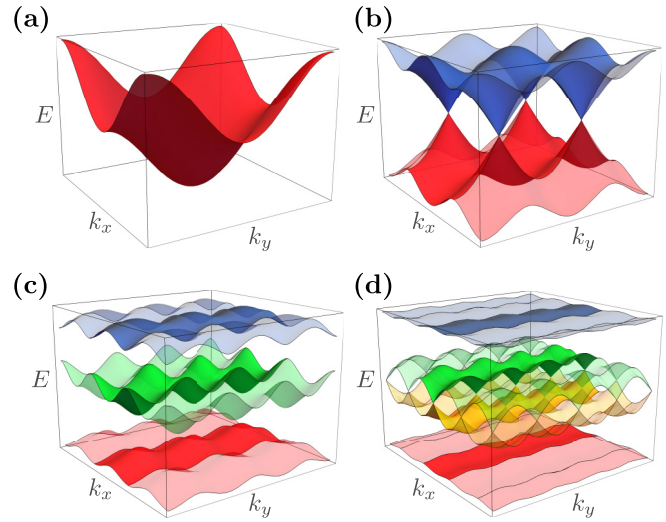

FIG. 3. Band structures for different phases in the soluble limit of the model. The range of the plot is the full Brillouin zone BZ : $-\pi \leqslant k_x, k_y < \pi$, with the darker section indicating the reduced Brillouin zone $\mathrm{rBZ} = \mathrm{BZ} \cap \{k_x \in [-\pi/q, \pi/q)\}$ for the flux $\varphi = 2\pi p/q$. (a) $\varphi = 0$, (b) $\varphi = \pi$, (c) $\varphi = 2\pi/3$, (d) $\varphi = \pi/2$.

where $Q_{\mathbf{r}} = e^{i\vartheta}$ is satisfied ($P_{\mathbf{r}}^{(\vartheta)} \equiv \frac{1}{N}\sum_{j=0}^{N-1}[Q_{\mathbf{r}}e^{-i\vartheta}]^j$):

$$|\mathrm{GS}\rangle = \left[\prod_{\mathbf{r}} P_{\mathbf{r}}^{(\vartheta)}\right]|\varphi\rangle_\sigma|\mathrm{FS}\rangle_c. \tag{11}$$

Here, $|\mathrm{FS}\rangle_c$ represents the fermionic ground state for the two-dimensional gauge-fixed lattice with Hamiltonian $\mathcal{H}_\varphi = \langle\varphi|\mathcal{H}_w|\varphi\rangle$. The projection operator in effect creates a symmetric combination of all allowed gauge configuration, also referred to as a "quantum loop gas." The band structure in the fermionic sector consists of up to N distinct bands (see Fig. 3). If N is even, and depending on the value of the flux φ, bands may touch at half-filling, forming Dirac cones with a linear band dispersion. It is important to stress that the ground state described above does not break any crystalline translation and rotation symmetries.

B. Excitations

The single-particle fermionic excitations of the system can be obtained by inserting the fermionic operators to the *right* of the projectors while constructing the ground state:

$$|e;\mathbf{k},i\rangle = \left[\prod_{\mathbf{r}} P_{\mathbf{r}}^{(\vartheta)}\right]c_{\mathbf{k},i}^\dagger|\varphi\rangle_\sigma|\mathrm{FS}\rangle_c, \quad \mathbf{k} \notin \mathrm{FS} \tag{12a}$$

$$|h;\mathbf{k},i\rangle = \left[\prod_{\mathbf{r}} P_{\mathbf{r}}^{(\vartheta)}\right]c_{\mathbf{k},i}|\varphi\rangle_\sigma|\mathrm{FS}\rangle_c, \quad \mathbf{k} \in . \tag{12b}$$

Here, i indicates the band index. Analogously, one can construct multiparticle excitations by applying multiple fermionic operators. If the fermionic operators were instead applied to the left of the projectors, then the excitations would no longer be gapless since the fermionic operators do not commute with the star operators $Q_{\mathbf{r}}$ because of the density term $\hat{n}_{\mathbf{r}}$. These excitations are therefore gapped. In the simplest cases when $\theta = \frac{2\pi n}{N}$, $n = 0, \ldots N-1$, the associated cost in energy is

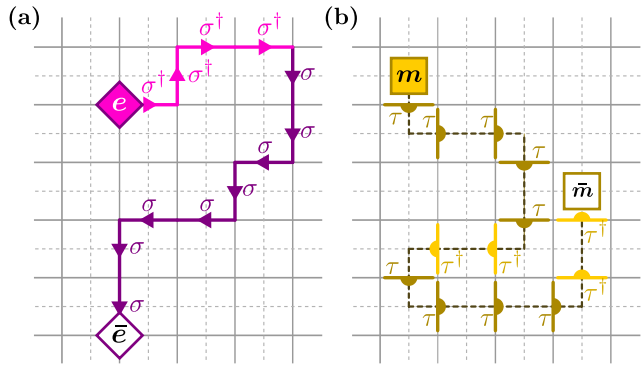

FIG. 4. The two gapped excitations on the $\mathbb{Z}_N$ toric code. The direction of the arrow (half-moon) indicates the appropriate choice for $\sigma_{\mathbf{r}_1,\mathbf{r}_2}(\tau_{\mathbf{p}_1,\mathbf{p}_2})$, pointing from $\mathbf{r}_1(\mathbf{p}_1)$ to $\mathbf{r}_2(\mathbf{p}_2)$. (a) An e particle-antiparticle pair, joined by a contour on the lattice (solid gray lines). (b) An m particle-antiparticle pair, joined by a contour on the dual lattice (dotted gray lines).

ηh, where $\eta = [1 - \cos(\frac{2\pi}{N})]$. This corresponds to the creation of an "e-particle" on the lattice, which can equivalently be created by electric string operators

$$\mathcal{W}^{(e)} = \prod_{\mathbf{b}_{\mathbf{r}_1,\mathbf{r}_2}\in\gamma} \sigma_{\mathbf{r}_1,\mathbf{r}_2}. \tag{13}$$

The notation $\sigma_{\mathbf{r}_1,\mathbf{r}_2}$ is necessary to specify the correct orientation; it corresponds to $\sigma^\dagger$ when $(\mathbf{r}_2 - \mathbf{r}_1) = \{\hat{x}, \hat{y}\}$ and σ otherwise [see Fig. 4(a)].

A key distinction is that the electric string operator $\mathcal{W}^{(e)}$ produces two e particles (for $N \neq 2$, a particle-antiparticle pair) at each end of the contour γ with total excitation energy $2\eta h$, whereas the fermionic operator to the left of the projector creates just one e particle coupled to the electron or hole.

There is another gapped excitation on top of the toric code ground state, the m particles, which reside on the dual lattice and are joined by τ insertions, analogous to the electric strings [Fig. 4(b)]

$$\mathcal{W}^{(m)} = \prod_{\mathbf{b}_{\mathbf{p}_1,\mathbf{p}_2}\in\gamma^*} \tau_{\mathbf{p}_1,\mathbf{p}_2}. \tag{14}$$

Also analogously, $\tau_{\mathbf{p}_1,\mathbf{p}_2}$ is oriented, corresponding to τ when $(\mathbf{p}_2 - \mathbf{p}_1) = \{\hat{x}, -\hat{y}\}$ and $\tau^\dagger$ otherwise.

In the regular toric code, both e and m particles excitations are static eigenstates, but in the fermionic toric code the m particles are not static due to their coupling to the Fermi sea. This peculiarity will be explored in more detail in Sec. V B, but we anticipate here, that, in the absence of fermions, the energetic cost of m particles in the simplest case $\phi = 2\pi n/N$, where $n = 0, 1, \ldots, N-1$, is ηK. The assumption introduced in the previous section, according to which the fermionic contribution to the ground-state energy is negligible, is equivalent to $w \ll K\eta$. Contrary to this, in the opposite limit where $0 < \eta K \lesssim w$, the ground states do break crystalline symmetries, even when represented projectively (i.e., symmetries modulo gauge transformations). The flux passing through the plaquettes is no longer homogeneous and is dominated by the fermionic sector. The fractional average flux is determined by the filling in the system: for a filling ρ, one expects the average flux density [86] to be $\varphi = 2\pi\rho$. This has been corroborated by Monte Carlo simulations [87] as well as a semianalytical study [63] in the special case $N = 2$. Relaxing the condition $\phi = 2\pi n/N$, we furthermore expect that the gapless fermionic sector influences the phase transitions between different sectors of Fig. 2(a) and leave detailed analyses of this regime for a general N to future studies.

We mention in passing here that the electric and magnetic string operators defined over closed contours instead of open are analogous to Wilson loop operators which play the role of nonlocal order parameters [88] for various topological phases hosted on this model.

IV. LUTTINGER-OSHIKAWA THEOREM

The phase ϕ of the plaquette term, Eq. (1a), alters the band structure of the fermionic sector and, more importantly, changes the volume of the Fermi surface. This appears to violate Luttinger's theorem [64], according to which the volume of the Fermi surface is only dependent on the fermionic filling ρ. For simplicity, and without loss of generality, in this section we concentrate on the spinless case N_f, in which ρ coincides with the density. In its modern formulation due to Oshikawa, a momentum balance argument [65] leads to Luttinger's theorem for conventional Fermi liquids (see more details below). However, a key step in the proof is assuming that momentum can only be carried by the quasiparticles of a conventional Fermi liquid. In our model, and generally in deconfining $\mathbb{Z}_N$ gauge theories, m particles are able to carry (angular) momentum, which leads to a modification in Oshikawa's proof [60,61]. We here generalize the Oshikawa proof to $\mathbb{Z}_N$ gauge theories, and illustrate the proof for the simplest $\mathbb{Z}_3$ case in the $|\varphi = 2\pi/3\rangle$ state [Fig. 3(c)]. We mention in passing that the generalization of Oshikawa's proof to SU(N) theories, of which $\mathbb{Z}_N$ is the center, was recently reported in Ref. [89].

Consider the model in a cylindrical setup with the specific gauge choice as shown in Fig. 5(a), at half-filling. We now adiabatically thread a physical flux of $2\pi/3$ through the cylinder. This flux can be absorbed into the internal gauge field by changing the bonds as shown in Fig. 5(b). The ground state describing the new lattice is related to the original ground state by a unitary transform

$$|\mathrm{GS}'\rangle = \mathcal{W}^{(m)}|\mathrm{GS}\rangle, \tag{15}$$

where $\mathcal{W}^{(m)}$ is the Wilson loop passing through the plaquettes.

One can show that the operator $T_y = \prod_{r\in\mathcal{C}} \omega^{\hat{n}_\mathbf{r}} Q^\dagger_\mathbf{r}$ translates the lattice by one unit in the y direction [Fig. 5(c)]. Applying this to $|\mathrm{GS}'\rangle$ gives

$$\begin{aligned} T_y|\mathrm{GS}'\rangle &= \prod_{\mathbf{r}\in\mathcal{C}} \omega^{\hat{n}_\mathbf{r}} Q^\dagger_\mathbf{r} (\mathcal{W}^{(m)}|\mathrm{GS}\rangle) \\ &= \prod_{\mathbf{r}\in\mathcal{C}} \exp\left(i\frac{2\pi}{3}\hat{n}_\mathbf{r}\right) \mathcal{W}^{(m)}|\mathrm{GS}\rangle \\ &= \exp\left(i\frac{2\pi L_x}{3}\rho\right)|\mathrm{GS}'\rangle, \end{aligned} \tag{16}$$

where we have assumed a homogeneous fermion filling $\rho = \langle\hat{n}_\mathbf{r}\rangle_{\mathbf{r}\in C}$.

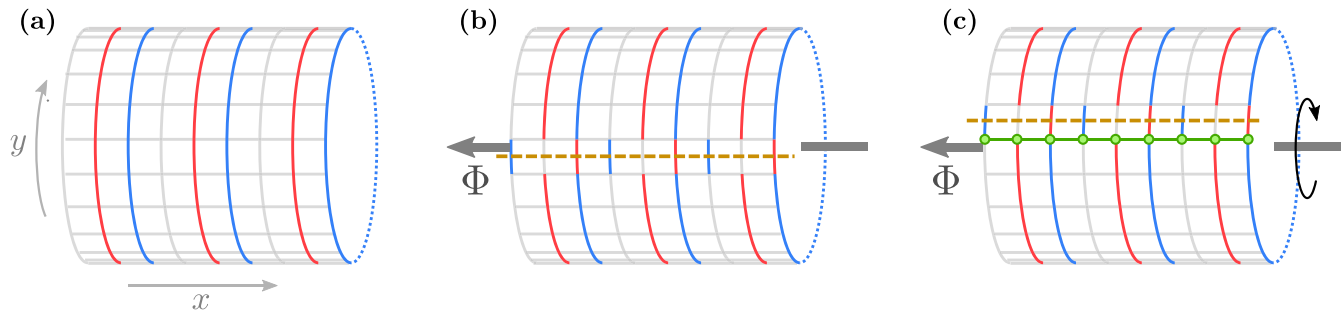

FIG. 5. (a) Modified Oshikawa's argument demonstrated for the $|\varphi = 2\pi/3\rangle$ flux state. (b) An adiabatic flux $\Phi = 2\pi/3$ through the system absorbed into the gauge field as a vison threading (orange). (c) The translation operator along the y axis T_y acting on the cylinder along the contour $\mathcal{C}$ (green).

Therefore, the momentum carried by the gauge field in this configuration [Eq. (16)] is $\Delta P = -\frac{2\pi L_x}{3}\rho$. This is the exact momentum imparted to the cylinder by the adiabatic flux insertion $\Delta P_{\text{tot}} = \Phi L_x \rho$, where $\Phi = -2\pi/3$. The momentum balance is accounted for and does not affect the fermionic distribution.

We now present a generalized relationship between fermion density and size of the Fermi surface. Arguments analogous to above hold for a flux insertion of $4\pi/3$, where the gauge sector absorbs the flux with two Wilson loops instead of one $[(\mathcal{W}^{(m)})^2|\text{GS}\rangle]$. The gauge field can thus carry away momenta in steps of $2\pi/3$. Adding this condition to the standard momentum balance calculation done before leads to the modified result (17):

$$\frac{V_{\text{FS}}}{(2\pi)^2} \pm \frac{1}{3} = \rho + p, \tag{17}$$

where $p \in \mathbb{Z}$. We see this is true at $\rho = \frac{1}{2}$, when the volume of the Fermi surface is $V_{\text{FS}} = (2\pi)^2/6$. Including the case where the flux is not threaded at all and entirely carried by the Fermi quasiparticles, the final relation is (in terms of a general N)

$$\frac{V_{\text{FS}}}{(2\pi)^2} = \rho \left(\text{mod } \frac{1}{N}\right). \tag{18}$$

It is of note that we arrived at this result without any knowledge of the band structure or details about the Fermi surface.

V. CORRELATORS AND DIAGRAMMATICS

In this section, we first study the correlators of fermions as well as σ insertions on the lattice and present a set of Feynman diagrams to graphically encode these correlators (see Appendix B). Subsequently, we discuss τ insertions.

A. Feynman rules for fermions and *e* particles

To evaluate an arbitrary imaginary-time-ordered ground-state correlator with $c_{\mathbf{r}}$, $c^\dagger_{\mathbf{r}}$, and $\sigma_{\mathbf{b}}$ with the general form

$$C(\{\mathbf{r}, \tau\}) = -\left\langle \mathcal{T}\left\{ \prod_n O^{(c)}_{\mathbf{r}_n}(\tau_n) \prod_m O^{(\sigma)}_{\mathbf{r}_m,\mathbf{r}'_m}(\tau_m) \right\} \right\rangle_{\text{GS}}. \tag{19}$$

Here, $O^{(c)}_{\mathbf{r}_n}(\tau_n) \in \{c_{\mathbf{r}_n}(\tau_n), c^\dagger_{\mathbf{r}_n}(\tau_n)\}$ and $O^{(\sigma)}_{\mathbf{r}_m,\mathbf{r}'_m}(\tau_m)$ is defined for nearest neighbor $\mathbf{r}_m$, $\mathbf{r}'_m$ as

$$O^{(\sigma)}_{\mathbf{r}_m,\mathbf{r}'_m} = \begin{cases} \sigma^\dagger & \text{for } \mathbf{r}'_m - \mathbf{r}_m = \hat{x}, \hat{y}, \\ \sigma & \text{for } \mathbf{r}'_m - \mathbf{r}_m = -\hat{x}, -\hat{y}. \end{cases} \tag{20}$$

To facilitate clear notation, we hereafter consider the simplest case $\theta = 0$:

(1) Draw $\circ$ for $c_{\mathbf{r}_n}(\tau_n)$, $\bullet$ for $c^\dagger_{\mathbf{r}_n}(\tau_n)$, and a solid line with an arrowhead for $O^{(\sigma)}_{\mathbf{r}_m,\mathbf{r}'_m}(\tau_m)$, pointing from $\mathbf{r}_m$ to $\mathbf{r}'_m$ [see Fig. 6(a)]. Higher powers of σ are indicated by multiple arrowheads.

(2) The "charge" $q_i \in \{1, \ldots, n\}$ is defined as the power of ω obtained from commuting $O_i \in \{O^{(c)}_{\mathbf{r}}, O^{(\sigma)}_{\mathbf{r},\mathbf{r}'}\}$ across $Q_{\mathbf{r}}$:

$$Q_{\mathbf{r}} O_i = \omega^{q_i} O_i Q_{\mathbf{r}}. \tag{21}$$

For n operators $O_1, \ldots, O_n$ at site $\mathbf{r}$ with times $\tau_1, \ldots, \tau_n$, respectively:

(i) The operators must satisfy charge neutrality modulo N,

$$\sum_{i=1}^{n} q_i = N\mathbb{Z}. \tag{22}$$

Note that $O^{(\sigma)}_{\mathbf{r}_1,\mathbf{r}_2}$ contributes to both sites $\mathbf{r}_1$ (with charge $+1$) and $\mathbf{r}_2$ (with charge -1).

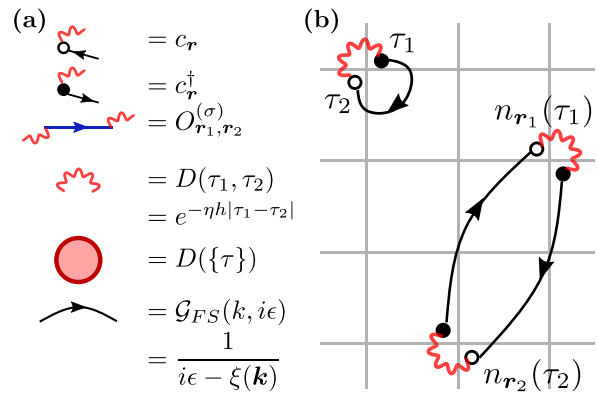

FIG. 6. (a) Feynman rules for calculating correlators. (b) The onsite fermionic Green's function (top left) and the polarization operator (right).

(ii) Connect operators on the same site by wavy lines. If there are more than two operators, encircle them. This corresponds to the exponential factor

$$\exp\left[h\sum_{i=1}^{n}\tau_{p(i)}\Re\left\{\omega^{-\sum_{j=1}^{i}q_{p(j)}}(1-\omega^{q_{p(i)}})\right\}\right], \tag{23}$$

where $p(i):\{1,\ldots,n\}\to\{1,\ldots,n\}$ is the index permutation that orders the times appropriately

$$\tau_{p(1)}>\tau_{p(2)}>\cdots>\tau_{p(n-1)}>\tau_{p(n)}. \tag{24}$$

For only two operators, this takes the simple form $D(\tau_1,\tau_2)=e^{-\eta h|\tau_1-\tau_2|}$, where we remind the reader of the excitation energy $\eta h=[1-\cos(\frac{2\pi}{N})]h$ of an e particle.

(3) Replace all arrowheads with their expectation value $\langle\varphi|O^{(\sigma)}_{\mathbf{r}_1,\mathbf{r}_2}|\varphi\rangle$.

(4) Connect all $\circ,\bullet$ in all possible combinations in accordance with the standard rules for fermionic diagrammatics, with solid lines representing the fermionic Green's function

$$\begin{aligned}G_{\mathrm{FS}}(\mathbf{r}_1,\mathbf{r}_2;\tau)&=-\langle\mathrm{FS}|\mathcal{T}\left[\bar{c}_{\mathbf{r}_1}(\tau)\bar{c}^{\dagger}_{\mathbf{r}_2}(0)\right]|\mathrm{FS}\rangle\\&=-\langle\mathrm{FS}|\mathcal{T}\left[e^{\mathcal{H}_\varphi\tau}c_{\mathbf{r}_1}e^{-\mathcal{H}_\varphi\tau}c^{\dagger}_{\mathbf{r}_2}\right]|\mathrm{FS}\rangle,\end{aligned}$$

where the bar above the operator indicates time evolution with respect to $\mathcal{H}_\varphi$ only.

The simplest correlator one can calculate is the two-point Green's function [Fig. 6(b)]: $\mathcal{G}(\mathbf{r}_1,\mathbf{r}_2;\tau)=-\langle\mathcal{T}c^{\dagger}_{\mathbf{r}_1}(\tau)c_{\mathbf{r}_2}(0)\rangle=\delta_{\mathbf{r}_1,\mathbf{r}_2}e^{-\eta h|\tau|}\mathcal{G}_{FS}(\mathbf{r}_1,\mathbf{r}_1;\tau)$. The ultralocal correlator is a consequence of the fact that e particles do not move in the integrable limit of the toric code. In the frequency representation,

$$\mathcal{G}(z)=\int(dk)\frac{1}{z-\xi_0(\mathbf{k})-\mathrm{sign}[\xi_0(\mathbf{k})]\eta h}, \tag{25}$$

where $\xi_0(\mathbf{k})=-2w[\cos(k_x)+\cos(k_y)]$ is the dispersion relationship for the zero-flux state and $(dk)=d^2k/(2\pi)^2$. The e particles (cf. Sec. III B) effectively create a gapped density of states, represented by the above equation. However, two-particle correlators in the particle-hole channels display regular Fermi-liquid behavior. For example, the polarization operator [Fig. 6(b)] is gapless since the e-particle propagator at each site evaluates to $D(\tau_i-\tau_i)=1$. This drastically different behavior of single and multiparticle correlators is characteristic of an orthogonal metallic phase [56], also referred to as a deconfined Fermi-liquid phase [90] due to the presence of both a large Fermi surface as well as fractionalized excitations. In contrast to the case $N=2$, $\mathbb{Z}_N$ orthogonal metals with $N>2$ have gapped two-particle correlators in the particle-particle channel, effectively preventing a Cooper instability.

B. Insertion of *m* particles

Unlike the insertion of the σ operators which commute with the fermionic part of the Hamiltonian (1c), the τ operators do not $[\tau_{\mathbf{b}},\mathcal{H}_w]\neq 0$. As a consequence, insertion of τ operators (i.e., insertion of m particles) triggers an Anderson orthogonality catastrophe, which we shall now explore. We mention in passing that a similar interplay of local spontaneous flux insertions with gapless fermionic modes is of fundamental importance in the physics of U(1) and Kitaev quantum spin liquids [91] as well as complex Kondo impurity systems [92].

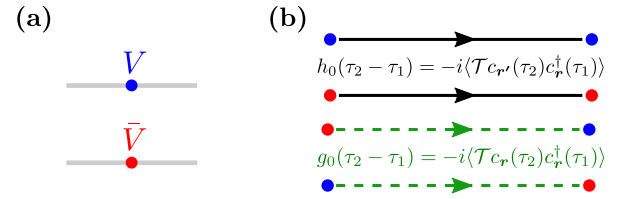

FIG. 7. (a) The two vertices in the perturbative expansion, $V=\frac{w}{2}(1-\omega)$ and $\bar{V}=\frac{w}{2}(1-\bar{\omega})$. (b) The two sets of propagators; g_0 joins two different vertices and h_0 joins vertices with the same colors.

We start by finding the τ-τ correlator corresponding to placing m particles at adjacent sites at time 0 and removing them at time t. (We switch to real time here momentarily to avoid confusion between $\tau_{\mathbf{b}}$, the clock operator, and τ, the imaginary time, and to remain consistent with previous literature; we will return to imaginary time at the end). One obtains an energy shift from the plaquettes $\mathcal{H}_K$, analogous to the σ insertions, but one gets an additional term from the fermionic contribution,

$$\begin{aligned}\mathcal{G}(\mathbf{b},t)&=-i\langle 0|\mathcal{T}\{\tau^{\dagger}_{\mathbf{b}}(t)\tau_{\mathbf{b}}(0)\}|0\rangle\\&=\underbrace{-i\langle\mathrm{FS}|\mathcal{T}\,\exp\left\{-i\int_0^{|t|}dt'\,\hat{V}(t')\right\}|\mathrm{FS}\rangle}_{\mathcal{G}'_{\mathrm{FS}}(\mathbf{b};t)}\\&\quad\times\exp(-2i\eta K|t|),\end{aligned} \tag{26a}$$

$$\hat{V}(t)=\frac{w}{2}(1-\omega)c^{\dagger}_{\mathbf{r}_1}(t)c_{\mathbf{r}_2}(t)+\mathrm{H.c.}, \tag{26b}$$

where $\mathbf{r}_1,\mathbf{r}_2$ are the sites corresponding to the bond $\mathbf{b}$. One must note that due to the translational and fourfold rotational symmetry of the 0-flux state, the choice of bond is irrelevant. The propagator $\mathcal{G}'_{\mathrm{FS}}$ corresponds to scattering from a time-dependent perturbation $\hat{V}(t)$ of the bond $\mathbf{b}$. This form is analogous to the x-ray edge problem [93,94], where the propagator gains not only an energy shift but also a transient part that results in a power-law decay at large times. Our propagator, however, differs in one key point: namely, the potential is not onsite but between neighboring sites.

Treating the potential perturbatively produces a set of connected and disconnected cycles, which can be summed using the linked cluster expansion [94] in two sets of complex vertices [$V\equiv\frac{w}{2}(1-\omega),\bar{V}$] and two types of propagators (see Fig. 7)

$$h_0(\tau_2-\tau_1)=-i\langle\mathcal{T}c_{\mathbf{r}_2}(\tau_2)c^{\dagger}_{\mathbf{r}_1}(\tau_1)\rangle=-i\langle\mathcal{T}c_{\mathbf{r}_1}(\tau_2)c^{\dagger}_{\mathbf{r}_2}(\tau_1)\rangle, \tag{27a}$$

$$g_0(\tau_2-\tau_1)=-i\langle\mathcal{T}c_{\mathbf{r}_1}(\tau_2)c^{\dagger}_{\mathbf{r}_1}(\tau_1)\rangle=-i\langle\mathcal{T}c_{\mathbf{r}_2}(\tau_2)c^{\dagger}_{\mathbf{r}_2}(\tau_1)\rangle. \tag{27b}$$

The solution can also be obtained in a nonperturbative fashion, following the method of Nozieres and de Dominicis [94,95]. The details of the calculation are relegated to Appendix C.

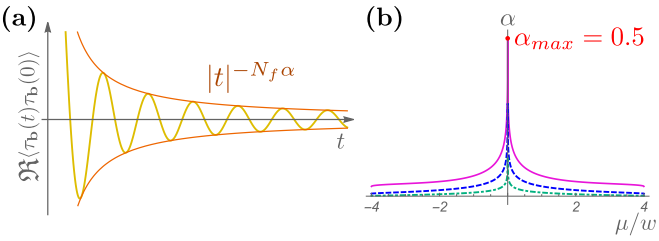

FIG. 8. (a) A schematic of the (real part of the) real-time τ-τ correlator (yellow), with a power-law envelope (orange). (b) Dependence of the power-law exponent α on the chemical potential μ for $N = 3$ (purple, solid), $N = 5$ (blue, dashed), and $N = 7$ (green, dotted dashed). At the van Hove singularity, all approach a maximum value of 0.5.

The result for the propagator is

$$\Re \ln \mathcal{G}'_{\rm FS}(t) = -N_f \underbrace{\left\{\left(\frac{\delta_1}{\pi}\right)^2 + \left(\frac{\delta_2}{\pi}\right)^2\right\}}_{\equiv\alpha} \ln(|t|) \tag{28}$$

with

$$\delta_i = \arctan\left\{\pi\left[\rho_0^h \Re V + (-1)^i \sqrt{|V|^2(\rho_0)^2 - \left(\mathrm{Im}V\,\rho_0^h\right)^2}\right]\right\}.$$

Here, we have returned to the general number N_f of internal degrees of freedom of the fermions, e.g., $N_f = 2$ due to spin.

As one can see, the factors δ_1, δ_2 depend on the local density of states (DOS), each acquiring a value of $\frac{\pi}{2}$ as the DOS approaches infinity, which occurs in the orthogonal metal phase at half-filling (cf. [96] for the orthogonality catastrophe at a van Hove singularity). In contrast, the DOS vanishes for half-filling in the orthogonal semimetal (OSM) phase (even N) and the orthogonality catastrophe term disappears. One should note that the τ-τ propagator acquires a phase shift from the energy shift due to the scattering potential, but an estimate of this requires nonanalytical methods. However, we can conclude that it is of the order of the bandwidth w since that is the only energy scale in the correlator, and since we work in the regime $K\eta \gg w$ we can ignore this shift safely.

The real-time propagator thus quickly oscillates on the scale $1/K\eta$ and its envelope slowly decays as $\mathcal{G}(t) \sim |t|^{-N_f\alpha}$, where the N_f accounts for the flavor degeneracy of the fermions. The exponent α depends on the chemical potential in the OM state (μ) as well as N [see Fig. 8(b)]. In imaginary time, the oscillation is replaced by exponential decay, which overshadows the power-law at scales beyond $(K\eta)^{-1}$.

VI. PERTURBATIONS AND INSTABILITIES

In this section, we add various perturbations to the soluble limit which introduce a finite string tension and discuss the instabilities of the orthogonal metal phase. In analogy to the previous section, we first discuss the impact of spontaneous σ insertions and subsequently of spontaneous τ insertions.

A. Spontaneous σ insertions: Kinetics of e particles, Luttinger surface, and Higgs transition

We now introduce a perturbation that delocalizes the e particles (wavy lines), which were previously confined to one vertex. We do this by introducing $\sigma_{\mathbf{b}}$ terms in the Hamiltonian

$$\mathcal{H}_J = -\frac{J}{2}\sum_{\mathbf{b}}(\sigma_{\mathbf{b}} + \sigma_{\mathbf{b}}^\dagger). \tag{29}$$

We first consider the orthogonal metal phase (zero-flux state $\langle\varphi = 0|\sigma_{\mathbf{b}}|\varphi = 0\rangle = 1$). The resummation of nonintersecting strings of σ insertions is given by

$$\mathbf{D}(\mathbf{r}_f, \mathbf{r}_i; i\omega) = D(i\omega)\delta_{\mathbf{r}_f,\mathbf{r}_i} + \frac{J}{2}\sum_{\langle \mathbf{r},\mathbf{r}_f\rangle}\left\langle O^{(\sigma)}_{\mathbf{r},\mathbf{r}_f}\right\rangle_0 \mathbf{D}(\mathbf{r}, \mathbf{r}_i; i\omega)D(i\omega), \tag{30}$$

where $D(i\omega) = \mathcal{F}\{e^{-h|\tau|\eta}\}(\omega) = 2\eta h/(\omega^2 + (\eta h)^2)$ and $\mathcal{F}$ denotes Fourier transform. The object $\mathbf{D}(\mathbf{r}_f, \mathbf{r}_i; i\omega)$ effectively describes the e-particle propagator.

In momentum space, this implies $\mathbf{D}(\mathbf{q}, i\omega) = D(i\omega) + J[\cos(q_x) + \cos(q_y)]D(i\omega)\mathbf{D}(\mathbf{q}, i\omega)$, giving us

$$\mathbf{D}(\mathbf{q}, i\omega) = \frac{2\eta h}{\omega^2 + \eta h\{\eta h - 2J[\cos(q_x) + \cos(q_y)]\}}. \tag{31}$$

Note that for $N = 2$, the propagator gains an extra factor of 2 since $O^{(\sigma)}_{\mathbf{r}_1,\mathbf{r}_2} = O^{(\sigma)}_{\mathbf{r}_2,\mathbf{r}_1}$ and the resummation gains an extra term (cf. [63] for the $\mathbb{Z}_2$ propagator). One can add a second perturbation to this: a fermionic Hamiltonian with small nearest-neighbor hopping. It should be noted that this perturbation is added on top of the existing Fermi sea

$$\mathcal{H}_t = -t\sum_{\langle \mathbf{r},\mathbf{r}'\rangle} c^\dagger_{\mathbf{r}} c_{\mathbf{r}'}. \tag{32}$$

The fermionic perturbation modifies the Green's function, with the resummation given by the equation

$$\mathbf{D}_t(\mathbf{r}_f, \mathbf{r}_i; i\omega) = \mathbf{D}(\mathbf{r}_f, \mathbf{r}_i; i\omega) + t\sum_{\mathbf{r}}\sum_{\langle \mathbf{r}',\mathbf{r}\rangle} \times \mathbf{D}(\mathbf{r}, \mathbf{r}_i; i\omega)\mathcal{G}_{\rm FS}(\mathbf{r}, \mathbf{r}')\mathbf{D}_t(\mathbf{r}_f, \mathbf{r}'; i\omega). \tag{33}$$

In momentum space,

$$\mathbf{D}_t(\mathbf{q}, i\omega) = \mathbf{D}(\mathbf{q}, i\omega) + \bar{t}\,\mathbf{D}(\mathbf{q}, i\omega)\mathbf{D}_t(\mathbf{q}, i\omega), \tag{34}$$

where $\bar{t} = 2t\ \mathcal{G}_{\rm FS}(r, r + \hat{e}_x)$. The new propagator is, therefore, analogously to Eq. (31) with the replacement $J \to (J + \bar{t})$.

1. *Luttinger surface of Green's function zeros*

As outlined in the Introduction, it is a question of current interest to understand the nature and occurrence of zeros in the electronic Green's function [72] of strongly correlated systems. Specifically, these zeros, which can be understood as poles of the self-energy, contribute to the thermodynamics [73] and topology [74–76] very much alike conventional quasiparticles in Fermi liquids and noninteracting electronic systems. At the same time, it is apparent that the low-energy thermodynamics of orthogonal (semi)metals is equivalent to the thermodynamics of their nonorthogonal counterparts. In this section, we demonstrate a connection between orthogonal metals and the occurrence of zeros in the Green's function. However, the Luttinger surface of zeros is unrelated to the density count.

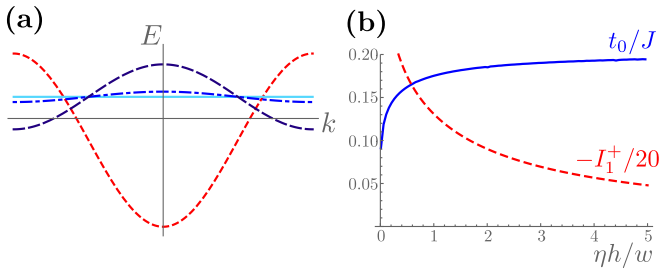

FIG. 9. (a) Schematic representation of the dispersion relation of orthogonal fermions (red, dotted), and Green's function zeros [Eq. (36)] for $t_0 = 0$ (light blue), $0 < 4t_0 < \mu_0$ (blue, dotted dashed), $\mu_0 < 4t_0$ (dark blue, dashed). (b) Dimensionless parameters entering t_0 and $\mathcal{Z}$ [cf. Eq. (36)] as a function of $\eta h/w$.

To this end, we calculate the fermionic Green's function

$$\mathcal{G}(\mathbf{p}, i\epsilon) = a^2 \int_{\mathrm{BZ}} (dq) \int (d\omega) \mathbf{D}(\mathbf{q}, i\omega) G_{\mathrm{FS}}(\mathbf{p}+\mathbf{q}, i\epsilon + i\omega), \tag{35}$$

perturbatively in J and inside the gap of Eq. (25). Relegating details to Appendix D, we find

$$\mathcal{G}(\mathbf{p}, z) = -\frac{1}{\mathcal{Z}}[z + \zeta_0(\mathbf{p})], \tag{36a}$$

with a dispersion of zeros of the form

$$\zeta_0(\mathbf{p}) = -2t_0[\cos(p_x) + \cos(p_y)] - \mu_0, \tag{36b}$$

and

$$t_0 = -J \frac{\eta h}{8w} \frac{I_1^+ + 2\pi w/\eta h}{I_1^+} > 0, \tag{36c}$$

$$\mu_0 = -\frac{1}{\nu_0} \frac{n(\mu) - n(-\mu)}{I_1^+} = \mathrm{sign}(\mu)|\mu_0|, \tag{36d}$$

$$\mathcal{Z} = -(\eta h/\nu_0 a^2) I_1^+ > 0. \tag{36e}$$

Note that the "weight of zeros" $\mathcal{Z}$ has dimensions of energy squared. The dimensionless integral $I_1^+(\eta h/w)$ is plotted along with t_0 and a schematic representation of the dispersion of orthogonal fermions and of zeros in Fig. 9. Crucially we observe that the Luttinger count enclosed by zeros is completely unrelated to the Fermi surface of orthogonal metals. Indeed, in the integrable limit $J = 0$, the zeros of the Green's functions are dispersionless and reside at energy $z = \mu_0$, where μ_0 is a function of I_1^+ as well as the filling fraction of the orthogonal fermions $n(\mu)$. Small $t_0 < |\mu_0|/4$ does not lead to the appearance of a Luttinger surface. For larger t_0 the Luttinger surface appears, but, as mentioned, it is unrelated to the Fermi surface of fermions.

In addition to the Luttinger surface being unrelated to fermion density, there are multiple distinctions between the zeros occurring in this context as compared to earlier discussions in the literature. The main reason is that the Luttinger surface encountered here originates from the dispersion of "e" particles (rather than, e.g., from a self-energy in the fermionic Green's function). Luttinger's theorem is fulfilled by the count of poles of orthogonal electrons, corrected for the effect of visons, Eq. (18). While analogously to the situation discussed by Fabrizio [73] the present fractionalized metal displays

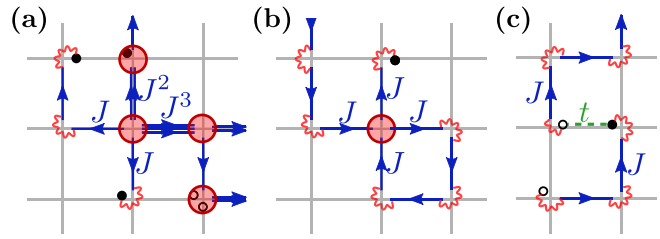

FIG. 10. Diagrams that contribute to the confinement-deconfinement transition. (a) The $\mathbb{Z}_N$ term (illustrated specifically for $\mathbb{Z}_7$). (b) The four-point self-interaction term. (c) The fermion-string interaction term.

Fermi-liquid thermodynamics, the distinction is that this thermodynamic response does not originate from the Luttinger surface but rather from the orthogonal fermions.

2. *Higgs transition*

The correlator $\mathbf{D}(\mathbf{q} = 0, i\nu = 0)$ represents the sum of open electric strings of all lengths. The singular behavior at $\eta h = 4(J + \bar{t})$ indicates condensation of e particles, corresponding to the confinement-deconfinement transition of the regular toric code. If $J + \bar{t}$ is increased further, the system undergoes a transition from an orthogonal metal to a regular Fermi liquid. At the critical point where confinement occurs, one can write the continuum theory as a $\mathbb{Z}_N$ lattice gauge theory coupled to fermions (cf. [56,63] for the cases $N = 2, 4$)

$$\mathcal{S} = \mathcal{S}_f + \mathcal{S}_b + \mathcal{S}_{\mathrm{IA}}, \tag{37a}$$

$$\mathcal{S}_b = \int d\tau\, d^2x\, \bar{\phi}\big[-\partial_\tau^2 - v^2\nabla^2 + r\big]\phi + u_0|\phi|^4 + u(\phi^N + \bar{\phi}^N), \tag{37b}$$

$$\mathcal{S}_f = \int d\tau\, d^2x\, \bar{\psi}[\partial_\tau + \epsilon(-i\nabla)]\psi, \tag{37c}$$

$$\mathcal{S}_{\mathrm{IA}} = \gamma \int d\tau\, d^2x\, \bar{\psi}\,[\cos(-i\partial_x) + \cos(-i\partial_y)]\,\psi|\phi|^2. \tag{37d}$$

The complex field ϕ (Grassmann field ψ) describes the fluctuations of the electric strings (fermions) near criticality [$\mathbf{D}(\mathbf{x}, \tau) = 2\eta h a^2 \langle\bar{\phi}(\mathbf{x}, \tau)\phi(0, 0)\rangle$, $\mathcal{G}_{\mathrm{FS}}(\mathbf{x}, t) = a^2\langle\bar{\psi}(\mathbf{x}, \tau)\psi(0, 0)\rangle$ and a is the lattice spacing]. A first-order time derivative does not occur given the quadratic frequency dependence of the resummed propagator (31). Observing Eq. (31), one can identify the constants $v^2 = \eta h[\eta h - 4(J + \bar{t})]$ and $r = \eta h(J + \bar{t})a^2$. Moreover, we have determined the four-point self-interaction vertex $u_0 \sim a^2 J^4/(\eta h)$ as well as the $\mathbb{Z}_N$ vertex $u \sim a^{N-2} J^N / h^{(\frac{N}{2}-1)}$ (cf. Appendix E). We emphasize that the fermionic interactions are added on top of the Fermi sea, so $\gamma \sim t$. Figure 10 illustrates some of the diagrams that contribute to the aforementioned transition.

The nature of the phase transition hinges on the value of N, as shown in Fig. 11. Note that for $N \geqslant 5$, the transition will be of U(1) type. We also remark that, contrary to the quasi-1D case, the Higgs transition is not expected to be preempted by a U(1) phase. This is because the Higgs transition stems from the toric code sector alone and intermediate U(1) phases are

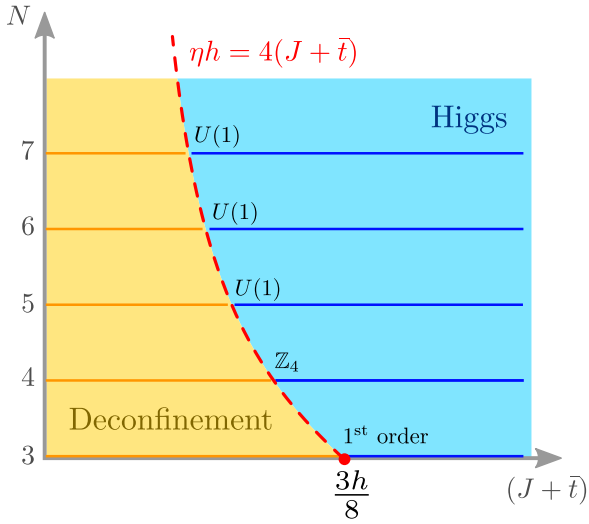

FIG. 11. Phase diagram representing the confinement-deconfinement transition for $N > 2$. The phase boundary (red) occurs at $\eta h = 4(J + \bar{t})$.

not permitted in two spatial dimensions (see Sec. VII for a review).

B. Spontaneous τ insertions: Hadron formation

While in the previous section we studied the effect of statistically appearing e particles (obtained by σ insertions), we here study the effect of m particles. To this end we add

$$\mathcal{H}_g = -\frac{g}{2}\sum_{\mathbf{b}}(\tau_{\mathbf{b}} + \tau_{\mathbf{b}}^\dagger) \tag{38}$$

to the basic Hamiltonian (1), but set $J = t = 0$.

As we already saw, insertion of τ results in an Anderson orthogonality catastrophe, such that the m-particle dynamics in the presence of fermions is very different from the dynamics of e particles [Eq. (31)]. Technically, this is reflected in a much less straightforward computation as the previous section.

As a remedy to avoid the orthogonality catastrophe physics, it is physically favorable to bunch fermions into charge-neutral N-particle bound states ("hadrons"). Here, we present details on the hadron formation under the assumption of $N_f = N$ fermion flavors. For simplicity, we concentrate on the limit of large h, $\phi = 0$ and low fermion filling (so that the Fermi surface is given by a circle and umklapp effects generating order in the particle-hole channels [25] is disabled.)

We first focus on the limit of low magnetic string tension $g \ll \eta K$. Further, since we are already working in the limit $\eta K \gg w$, the orthogonal fermions are relatively slow as compared to the m particles introduced with the perturbation. These m particles induce an attractive interaction within the fermions, and for large enough g, create an instability in the OM phase. The instability can be identified as a singularity in the N-particle interaction channel, the leading contribution to which is obtained from a "ladder" resummation (see Fig. 12) (for $N = 2$, the calculation is equivalent to that of the Cooper instability).

The bare interaction induced by the m particles is characterized by $\mathcal{V}$. We can estimate $\mathcal{V}$ by finding the effective

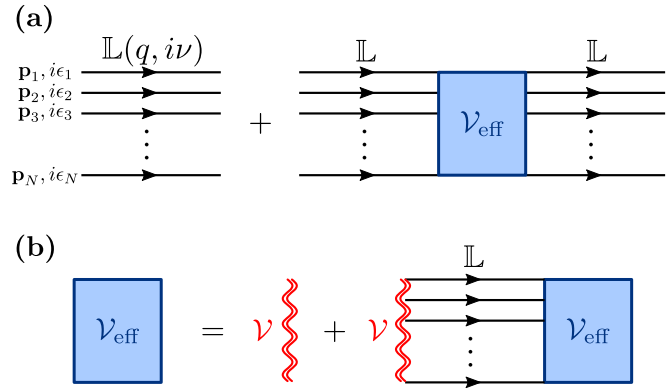

FIG. 12. Ladder resummation of the N-particle propagator. (a) The resummation in terms of the noninteracting ladder $\mathbb{L}(\mathbf{q} = \sum_j \mathbf{p}_j, i\nu = \sum_j i\epsilon_j)$ and the effective interaction vertex $\mathcal{V}_{\text{eff}}$. (b) The Bethe-Salpeter equation defining the effective interaction vertex in terms of $\mathbb{L}$ and the bare interaction $\mathcal{V}$.

N-fermion hopping amplitude from perturbing around the OM ground state, treating g as a small parameter in the partition function

$$\frac{Z}{Z_0} = \mathrm{Tr}\left[\mathcal{T}\exp\left(-\int d\tau\, \mathcal{H}_g(\tau)\right)\right]. \tag{39}$$

Ignoring higher-order contributions corresponding to m-particle insertions in loops, the first nonzero contribution to the hopping arises from Nth order in g, with an amplitude of $(gw)^N/(\Delta E_m)^{2N-1}$, ΔE_m being the energy gap of the m particles. While at the integrable limit this is simply ηK, it gets modified to $\sqrt{\eta K(\eta K - 4g)}$ as one approaches m-particle confinement [analogous to e particles, cf. Eq. (31)].

Appendix F presents the details of the N-ladder correlator as well as the calculations of the critical temperature at which the hadron instability sets in, given by

$$T_h(g \ll K) = T_h^{(0)}\left(1 - \frac{1}{v\alpha_N(0)}\right), \tag{40}$$

where $\alpha_N(0) = \int_0^1 \prod_i^N (dx_i)(\sum_i^N x_i)^{-1}$ is finite for all $N > 2$ and behaves as $2/N$ in the large-N limit. The dimensionless interaction v is a function of the bare interaction $\mathcal{V}$ and the chemical potential μ (above the bottom of the band). The scaling of dimensionless v as a function of g, K, w as well as the chemical potential is

$$v(g/K) \sim \left(\frac{g}{\Delta E_m}\right)^N \left(\frac{w}{\Delta E_m}\right)\left(\frac{\mu'}{\Delta E_m}\right)^{N-2}. \tag{41}$$

Here and henceforth, the dashed quantity μ' indicates the chemical potential above zero filling, as opposed to the μ in Eq. (1) which is zero at half-filling. As g/K increases, one sees that the proposed transition always occurs before the condensation of m particles (see Fig. 13), supporting the hypothesis that the m-particle dynamics result in a retarded attractive interaction and subsequent hadron instability. As g approaches $\eta K/4$, T_h approaches a maximum value $T_h^{(0)} \sim \mu'/N$.

In the opposite limit, deep in the confining phase for m particles ($g \gg \eta K$) the $\mathbb{Z}_N$ clock variables on the lattice align in the τ basis which renders them disordered in the σ basis.

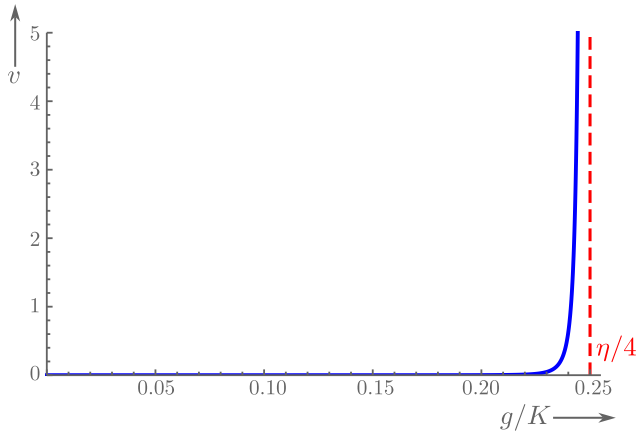

FIG. 13. Estimate for the dimensionless hadron interaction v [Eq. (41)], varying with g/K (blue). The plot has been constructed for $N = 4$, $w/\eta K = 0.3$, and $\mu/w = 0.3$. v has a vertical asymptote at $\eta K = 4g$ (red), the point at which m-particle condensation occurs.

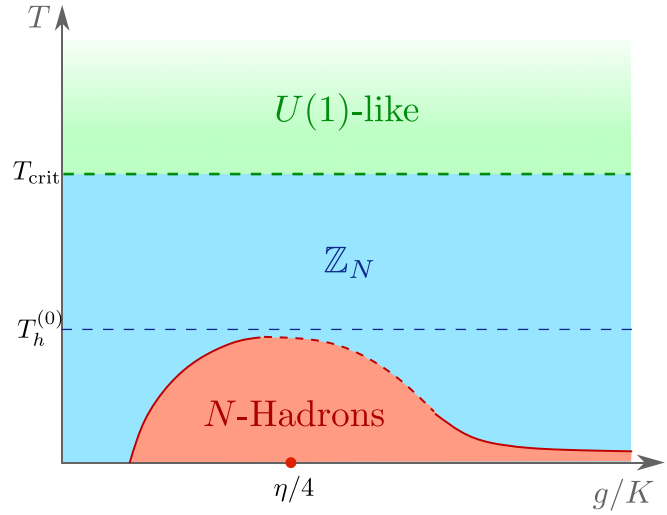

FIG. 14. Schematic phase diagram of temperature T vs g/K for small fermion filling showing the dome of hadron formation (red) buried in the $\mathbb{Z}_N$ phase (blue). The point $\eta K = 4g$ indicates the zero-temperature confinement-deconfinement transition for the m particles. At higher temperatures $T > T_{\rm crit}$, our RG-flow analysis suggests U(1)-like behavior (green).

This results in an insulating phase for the fermions for low temperatures. One can carry out perturbation theory on the new ground state where $\tau_{\mathbf{b}} = 1$, treating w as a small parameter,

$$\frac{Z}{Z_0} = \mathrm{Tr}\left[\mathcal{T}\,\exp\left(-\int d\tau\,\mathcal{H}_w(\tau)\right)\right]. \tag{42}$$

Expanding this expression to Nth order in w produces an effective nearest-neighbor hopping of $[c^\dagger_{\mathbf{r}}]^N[c_{\mathbf{r}'}]^N$, with an amplitude of the order $t_{\rm eff} \sim w^N/g^{N-1}$. In this regime, assuming that the N hadrons show bosonic statistics, i.e., $N \in 2\mathbb{N}$, the condensation sets in as a Berezinskii-Kosterlitz-Thouless (BKT) transition (see [25] for $N = 2$). One can then utilize BKT theory to estimate the transition temperature T_h in this regime

$$T_h(g \gg K) = T_{\rm BKT} \sim t_{\rm eff}\, n_b a^2, \tag{43}$$

where n_b is the boson density $[\sim(\mu/w)/N]$ and a the lattice spacing. This calculation suggests that the temperature T_h develops a tail with a power-law decay ($\sim\frac{1}{g^{N-1}}$), tapering off for large g/K.

In the regime between confinement and deconfinement of the magnetic sector ($g \sim \eta K$), one needs numerical tools to establish the exact phase boundary, but one expects to see a dome of N-hadron instability in the phase diagram as shown in Fig. 14, with the apex of the dome bounded above by the critical temperature $T_h^{(0)}$. A similar dome of superconductivity has been strongly evidenced for $N = 2$ in Ref. [25] using quantum Monte Carlo techniques, yet for $N = 2$ the hadron formation occurs at infinitesimal g/K.

We leave a remark in passing here that interactions between these N hadrons can lead to formation of higher-order aggregates that are more energetically favorable, like the formation of $2N$ hadrons with bosonic statistics for odd N, which can form condensates unlike their counterparts with fermionic statistics. This requires further analysis and will be dealt with in future studies.

VII. ABSENCE OF A U(1) PHASE

In the previous section we have argued that the confinement-deconfinement transition of the $\mathbb{Z}_N$ gauge theory with fermions is buried under a dome of hadron formation (in the case $N = 2$: a dome of superconductivity). Yet, one could have also expected that an intermediate U(1) phase occurs between the two phases, or might at least be stabilized by additional interactions in the Hamiltonian. In this section, we provide arguments why this is not the case. Instead, we here show that in $2 + 1$ dimensions [$(2 + 1)$D], QED coupled to a Fermi surface is a renormalization group fixed point which is unstable to $\mathbb{Z}_N$ perturbations. According to these results, it is strictly speaking not possible to emulate U(1) LGTs by finite Hilbert space $\mathbb{Z}_N$ approximants. However, we show that U(1) physics may persist at intermediate system sizes smaller than the length scales at which N-hadron bound states may be observed.

We first summarize the situation in the absence of fermionic matter fields, where indeed an intermediate U(1) phase occurs in one spatial dimension, but not in 2D. This can be understood as follows: While in $D = 1 + 1$ and large N, terms breaking U(1) symmetry down to $\mathbb{Z}_N$ are renormalization group (RG) irrelevant near the transition [31], such a mechanism is disallowed for $D = 2 + 1$. Indeed, in the dual (gauge theory) language, the disorder-order transition corresponds to a deconfinement-confinement transition. At the same time, compact QED_3 without matter fields is always in a confining phase, which implies that any putative U(1) phase would ultimately gap out at longest distances [97]. What, however, if the $\mathbb{Z}_N$ gauge theory in $D = 2 + 1$ is coupled to fermionic matter fields? Indeed, in contrast to the pure gauge theory, it is common knowledge that compact QED_3 coupled to a Fermi surface remains gapless [34–39]. Analogously to the logic applied in $(1 + 1)$D, we here study the effect of terms

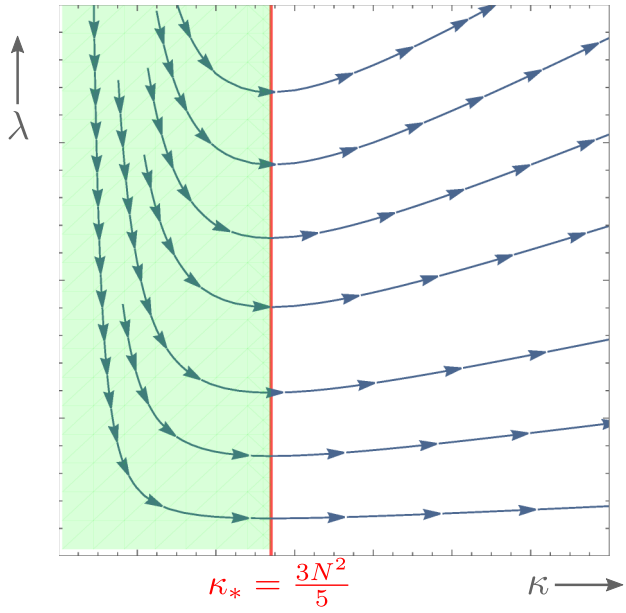

FIG. 15. A schematic of the flow of of the constants κ, λ under the renormalization group procedure. System scales corresponding to the green region can approximate U(1) order, where $\kappa < \frac{3N^2}{5}$.

breaking U(1) symmetry down to $\mathbb{Z}_N$ in a renormalization group treatment.

We here study the renormalization group flow for a $\mathbb{Z}_N$ perturbation added to the non-Fermi-liquid theory obtained by coupling a degenerate Fermi gas with N_f-fold flavor degeneracy to QED_3 gauge fluctuations (see Appendix G 2 for details). The flow equations are

$$\frac{d\kappa}{d\ \ln b} = 6\kappa, \tag{44a}$$

$$\frac{d\lambda}{d\ \ln b} = \left(5 - \frac{3N^2}{\kappa}\right)\lambda, \tag{44b}$$

where the constant λ determines the strength of the $\mathbb{Z}_N$ perturbation locking the U(1) gauge field to N discrete angles and the constant $1/\kappa$ linearly enters the propagator of the U(1) gauge field (analogously to a stiffness in Berezinskii-Kosterlitz-Thouless theory). One sees that since κ is relevant, λ is bound to flow to relevancy and thus the $\mathbb{Z}_N$ perturbation breaks U(1) order in the system. Figure 15 plots the flow Eqs. (44a) and (44b). Although there is no $\mathbb{Z}_N$ order, one can see quasi-U(1) behavior at intermediate system scales, corresponding to the green region of the phase space where λ flows to irrelevancy. Using the starting value $\kappa \sim 1/N_f^2$, we have calculated the critical length scale L_{crit} up to which this behavior persists and its dependence on N as well as the number of fermion flavors N_f,

$$L_{\text{crit}} \sim l\left(\frac{N}{N_f}\right)^{\frac{1}{3}}, \tag{45}$$

where l is the UV length cutoff which can be estimated of the order of the Fermi wave vector. The critical length scale endows a corresponding critical temperature $T_{\text{crit}} \sim \mu(N_f/N)$ above which the U(1)-like behavior in the system persists (see Fig. 14). In the case $N_f = N$ studied in the previous section, it is ensured that the quasi-U(1) behavior persists only outside the N-hadron phase ($T_{\text{crit}} > T_h^{(0)}$)

We emphasize that our calculations are performed within the random-phase approximation (RPA) of fermions coupled to emergent photons in 2D. It has been argued that a combination of large N_f and an ϵ expansion justifies the existence of a phase described by this phenomenology [39]. However, in strictly two spatial dimensions, the infrared fixed point of QED_3 coupled to a Fermi surface is unknown. While we can not exclude a scenario in which λ is relevant at the non-Fermi-liquid RPA fixed point but irrelevant at the unknown physical infrared fixed point, such a scenario seems extremely unlikely.

VIII. DISCUSSION AND OUTLOOK

In summary, we have coupled a $\mathbb{Z}_N$ generalization of Kitaev's toric code to fermions, obtaining a solvable model for fermions coupled to a $\mathbb{Z}_N$ lattice gauge theory in $2+1$ dimensions. This model exhibits a rich phase diagram with exotic changes in the Fermi-surface topology, switching from an orthogonal metal phase to an orthogonal semimetal (for even N) or a band insulator (for odd N). The deconfining sector of the toric code admits momentum transfer through the gauge field, allowing violation of Luttinger's theorem without symmetry breaking. In the integrable limit, we have also developed a diagrammatic technique for correlators of fermions and "σ" insertions (corresponding to e particles). We furthermore studied correlators of "τ" insertions (corresponding to m particles), which trigger an orthogonality catastrophe effect and a power-law decay at long times in the m-particle propagator. We have found a closed form for this power-law exponent systematically using linked cluster expansions.

We next included perturbations to the integrable limit which delocalize e and m particles of the toric code. In the deconfining phase, the term delocalizing e particles generates a dispersive band of Green's function zeros. We have also studied the Higgs transition corresponding to the condensation of e particles. We predicted the position of the phase transition within mean-field theory and developed an effective field theory to investigate the critical behavior of the system at this transition beyond mean field. The terms dynamically delocalizing m particles (which correspond to a finite string tension) tend to induce a hadron instability resulting in the formation of gauge-neutral hadrons consisting of N particles. In the case of $N_f \geqslant N$ flavors of fermions we explicitly demonstrate that the hadron instability buries the confinement-deconfinement transition underneath a hadronic dome (superconductivity in the case $N = 2$). We finally address the question of the limit $N \to \infty$ to answer whether $\mathbb{Z}_N$ LGT are good emulators for QED. Concentrating on the case of a Fermi surface but far away from half-filling, we present RG arguments according to which QED is always unstable, i.e., $\mathbb{Z}_N$ LGTs do not have a U(1) gapless phase in the infrared. However, we argue that at intermediate energy scales $\mathbb{Z}_N$ LGTs with $N \gg 1$ can be good approximations to QED_3.

In conclusion, both recent advances in quantum materials and the advent of new programmable quantum emulators have generated practical interest in topological phases of $\mathbb{Z}_N$ gauge theories. Here we studied fermionic fields in this context allowing to shed light on the physics of Luttinger surfaces

of Green's function zeros and the problem of Fermi-surface reconstruction without symmetry breaking. Interesting problems for the future involve the interplay of topological band structures with deconfining lattice gauge theories and the search for deconfining phases in more microscopic models of materials. At the same time, many physically relevant questions for quantum emulator implementations of deconfining gauge theories remain unanswered, most importantly those addressing important aspects of experimental imperfections such as decoherence.

ACKNOWLEDGMENTS

It is a pleasure to thank S. Moroz, P. M. Bonetti, M. S. Scheurer, I. Sodemann, U. Seifert, D. Vilardi, and O. Zilberberg for useful discussions. K.R. thanks the Max-Planck-Institute for Solid State Research for hospitality and the German Academic Exchange Service (DAAD) for support via the Working Internships in Science and Engineering (WISE) program. E.J.K. thanks the Kavli institute for Theoretical Physics (KITP) for hospitality, where this work was partially completed. Thereby, this research was supported in part by Grant No. NSF PHY-2309135 to the KITP.

APPENDIX A: QUANTUM CLOCK MODEL TO $\mathbb{Z}_N$ TORIC CODE

In this Appendix we summarize the mapping of the $\mathbb{Z}_N$ gauge theory (with fermionic and bosonic matter fields) to the $\mathbb{Z}_N$ toric code model [1,63,85]

$$\mathcal{H} = \mathcal{H}_{\mathbb{Z}_N} + \mathcal{H}_{\rm QC} + \mathcal{H}_f,$$

$$\mathcal{H}_{\mathbb{Z}_N} = -\frac{K}{2}\sum_{\mathbf{p}}\prod_{\mathbf{e}\in\{\hat{x},-\hat{y}\}}\bar{\sigma}_{\mathbf{r}+\frac{1}{2}\mathbf{e}}\bar{\sigma}^{\dagger}_{\mathbf{r}-\frac{1}{2}\mathbf{e}} - \frac{g}{2}\sum_{\mathbf{b}}\bar{\tau}_{\mathbf{b}} + \text{H.c.}, \tag{A1a}$$

$$\mathcal{H}_{\rm QC} = -\frac{J}{2}\sum_{\mathbf{r},\mathbf{e}\in\{\hat{x},\hat{y}\}}\bar{\sigma}_{(\mathbf{r}+\frac{1}{2}\mathbf{e})}\varsigma^{\dagger}_{\mathbf{r}}\varsigma_{\mathbf{r}+\mathbf{e}} - \frac{h}{2}\sum_{\mathbf{r}}\boldsymbol{\tau}_{\mathbf{r}} + \text{H.c.}, \tag{A1b}$$

$$\mathcal{H}_f = -\frac{w}{2}\sum_{\mathbf{r},\mathbf{e}\in\{\hat{x},\hat{y}\}}\bar{\sigma}_{(\mathbf{r}+\frac{1}{2}\mathbf{e})}f^{\dagger}_{\mathbf{r},\alpha}f_{\mathbf{r}+\mathbf{e},\alpha} + \text{H.c.} \tag{A1c}$$

$\mathcal{H}_{\rm QC}$ is the usual quantum clock Hamiltonian, with the interaction term modified with the addition of $\bar{\sigma}_{\mathbf{b}}$ to couple it to the gauge field.

Both sets of operators obey the algebra

$$\bar{\sigma}_{\mathbf{b}}\bar{\tau}_{\mathbf{b}'} = (\omega)^{\delta_{\mathbf{b},\mathbf{b}'}}\bar{\tau}_{\mathbf{b}'}\bar{\sigma}_{\mathbf{b}}, \tag{A2a}$$

$$\varsigma_{\mathbf{r}}\boldsymbol{\tau}_{\mathbf{r}'} = (\omega)^{\delta_{\mathbf{r},\mathbf{r}'}}\boldsymbol{\tau}_{\mathbf{r}'}\varsigma_{\mathbf{r}}, \tag{A2b}$$

where $\omega = e^{2\pi i/N}$, the Nth root of unity. The model has a local $\mathbb{Z}_N$ symmetry at each site generated by the operator $\bar{Q}_{\mathbf{r}}$:

$$\bar{Q}_{\mathbf{r}} = \underbrace{\omega^{\hat{n}_{\mathbf{r}}}\boldsymbol{\tau}_{\mathbf{r}}}_{\text{matter}}\underbrace{\prod_{\mathbf{e}\in\{\hat{x},\hat{y}\}}\bar{\tau}_{\mathbf{r}+\frac{1}{2}\mathbf{e}}\bar{\tau}^{\dagger}_{\mathbf{r}-\frac{1}{2}\mathbf{e}}}_{\text{gauge}}. \tag{A3}$$

To fix the local charge, we impose Gauss' law on the physical subspace

$$\bar{Q}_{\mathbf{r}}|\text{Phys}\rangle = |\text{Phys}\rangle. \tag{A4}$$

We thus make the replacement $\boldsymbol{\tau}^{\dagger}_{\mathbf{r}} \to \prod_{\mathbf{e}\in\{\hat{x},\hat{y}\}}\omega^{\hat{n}_{\mathbf{r}}}\bar{\tau}_{\mathbf{r}+\frac{1}{2}\mathbf{e}}\bar{\tau}^{\dagger}_{\mathbf{r}-\frac{1}{2}\mathbf{e}} (\equiv Q_{\mathbf{r}})$. We also enforce the unitary gauge on the physical subspace:

$$\varsigma_{\mathbf{r}}|\text{Phys}\rangle = |\text{Phys}\rangle. \tag{A5}$$

Finally, we replace the terms in the Hamiltonian with gauge-invariant quantities:

(1) $\mathcal{W}^{(e)}_{\gamma_{\mathbf{r},\mathbf{r}'}} = \varsigma^{\dagger}_{\mathbf{r}}[\prod_{\mathbf{r}_i\in\gamma}\bar{\sigma}_{\mathbf{r}_i,\mathbf{r}_{i+1}}]\varsigma_{\mathbf{r}'} \equiv \prod_{\mathbf{r}_i\in\gamma}\sigma_{\mathbf{r}_i,\mathbf{r}_{i+1}}$,

(2) $\bar{\tau}_{\mathbf{b}} \equiv \tau_{\mathbf{b}}$,

(3) $c_{\mathbf{r},\alpha} = \varsigma^{\dagger}_{\mathbf{r}}f_{\mathbf{r},\alpha}$,

giving us the gauge-fixed Hamiltonian

$$\begin{aligned}\mathcal{H} = &-\frac{K}{2}\sum_{\mathbf{p}}\prod_{\mathbf{e}\in\{\hat{x},-\hat{y}\}}\sigma_{\mathbf{r}+\frac{1}{2}\mathbf{e}}\sigma^{\dagger}_{\mathbf{r}-\frac{1}{2}\mathbf{e}} - \frac{g}{2}\sum_{\mathbf{b}}\tau_{\mathbf{b}} + \text{H.c.}\\ &-\frac{h}{2}\sum_{\mathbf{r}}\underbrace{\omega^{\hat{n}_{\mathbf{r}}}\prod_{\mathbf{e}\in\{\hat{x},\hat{y}\}}\tau_{\mathbf{r}+\frac{1}{2}\mathbf{e}}\tau^{\dagger}_{\mathbf{r}-\frac{1}{2}\mathbf{e}}}_{Q_{\mathbf{r}}} - \frac{J}{2}\sum_{\mathbf{r}}\sigma_{\mathbf{r}} + \text{H.c.}\\ &-\frac{w}{2}\sum_{\mathbf{r},\mathbf{e}\in\{\hat{x},\hat{y}\}}c^{\dagger}_{\mathbf{r},\alpha}\sigma_{(\mathbf{r}+\frac{1}{2}\mathbf{e})}c_{\mathbf{r}+\mathbf{e},\alpha} + \text{H.c.}\end{aligned} \tag{A6}$$

This concludes the argumentation exposed in Sec. II B of the main text.

APPENDIX B: DERIVATION OF FEYNMAN RULES

In this Appendix we derive the Feynman rules presented in Sec. V A. To this end, consider Eq. (19) with the Heisenberg picture time evolution $O(\tau) = e^{H\tau}Oe^{-H\tau}$:

(i) Write $|\text{GS}\rangle$ as $\prod_{\mathbf{r}}\hat{P}^{(0)}_{\mathbf{r}}|\varphi\rangle|\text{FS}\rangle$. Commuting the projector on the left across to the other side, one sees that the charge q_i on each site must be conserved modulo N for the product of projectors to not vanish. This gives Feynman rule 2. This implies that two fermionic operators must be joined by a string of oriented σ insertions, and equivalently that σ insertions must either be closed loops or terminate in one (or one modulo N) fermionic operator.

(ii) For an operator $O_{\mathbf{r}}$ with charge q_i, the explicit time evolution is $O_{\mathbf{r}}(\tau) = e^{\mathcal{H}_h\tau}e^{\mathcal{H}_w\tau}O_{\mathbf{r}}e^{-\mathcal{H}_w\tau}e^{-\mathcal{H}_h\tau} = \bar{O}_{\mathbf{r}}(\tau)\exp[\frac{h}{2}(1-\omega^q)Q_{\mathbf{r}}\tau + \text{H.c.}]$, where q is the charge of the operator O and $\bar{O}(\tau)$ indicates time evolution with respect to the fermionic part only.

(iii) At site $\mathbf{r}$, write the operators inside the correlator $C(\{\mathbf{r},\tau\}$ in time-ordered fashion. Replace all operators with the above time-evolution expression: $O_{\mathbf{r}}(\tau) = \bar{O}_{\mathbf{r}}(\tau)\exp[\frac{h}{2}(1-\omega^q)Q_{\mathbf{r}}\tau + \text{H.c.}]$. Commute the exponential terms to the right, making note of the charge of the subsequent operators ($Q_{\mathbf{r}}O_{\mathbf{r}'} = (\omega^q)^{\delta_{\mathbf{r},\mathbf{r}'}}O_{\mathbf{r}'}Q_{\mathbf{r}}$) and finally use $Q_{\mathbf{r}}|\text{GS}\rangle = |\text{GS}\rangle$ coupled with Feynman rule 2 to obtain the e-particle interaction term (23).

(iv) The only dependence on σ variables now lies in $\bar{O}(\tau)$, specifically in $\mathcal{H}_w$, and the σ insertions. The σ's can now be replaced with their expectation values on the gauge-fixed lattice ($\langle\varphi|\sigma_{\mathbf{r}}|\varphi\rangle$). This fixes the Hamiltonian $\mathcal{H}_w \to \mathcal{H}_\varphi$. For example, in the zero-flux orthogonal metal (OM) phase,

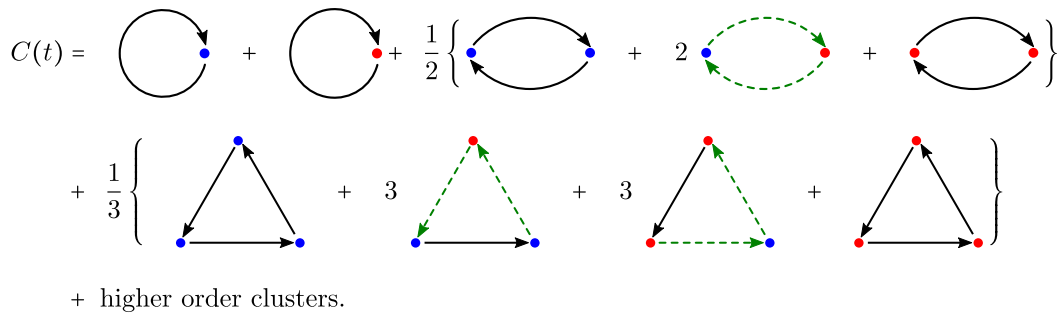

FIG. 16. The connected part of the transient operator $C(t)$ containing linked clusters of all orders.

$\langle\sigma_{\mathbf{r}}\rangle_0 = 1$ and H_w reduces to the regular 2D tight-binding Hamiltonian.

(v) The correlator has now been brought to the form $C(\mathbf{r},\tau) = \langle \mathrm{FS}|\mathcal{T}\{\bar{O}_{\mathbf{r}_1}(\tau_1)\bar{O}_{\mathbf{r}_2}(\tau_2)\ldots\bar{O}_{\mathbf{r}_n}(\tau_n)\}|\mathrm{FS}\rangle$. Now Wick's theorem can be applied.

The real-time Feynman rules are derived analogously, simply derived with a Wick rotation: $\tau \to it, |\tau_1 - \tau_2| \to i|t_1 - t_2|$.

APPENDIX C: NOZIERES–DE DOMINICIS SOLUTION

In this Appendix, we present details on the correlators of τ operators (m particles) in the presence of fermions, thereby complementing Sec. V B.

To understand the Nozieres–de Dominicis solution, we first lay out the perturbative method. The propagator $\mathcal{G}'_{\mathrm{FS}}(t'-t) = -i\langle\mathcal{T}\exp -i\int_t^{t'} d\tau\hat{V}(\tau)\rangle$ can be expanded in $V \equiv \frac{w}{2}(1-\omega)$ and $\bar{V}$ into a series of connected and disconnected diagrams with two types of vertices. This series can be resummed to an exponential of just the connected diagrams using the linked cluster theorem

$$\mathcal{G}'_{\mathrm{FS}}(t) = -ie^{C(t)}, \tag{C1}$$

where

$$C(t) = \left\langle \mathcal{T}\exp -i\int_0^t d\tau\hat{V}(\tau)\right\rangle_{\mathrm{connected}}. \tag{C2}$$

$C(t)$ is the sum of all closed-loop diagrams, as shown in Fig. 16 up to third order.

The diagrams above can be computed order by order, but only when the propagators in each diagram are nonsingular. While we concentrate on the case away from half-filling, where the fermionic Green's function is $g_0(t) \sim 1/wt$, we mention in passing that at the van Hove singularity the long-time behavior of the onsite propagator acquires an additional logarithm [$g_0(t) \sim \frac{\ln(t)}{wt}$] and each term in the expansion is more singular than the last. This amplifies the orthogonality catastrophe. However, it was shown [96] for the case of an abruptly appearing onsite potential that the phase shift obtained at half-filling is the same as determined using the naive extrapolating of the final result (as obtained for finite density of states) to the van Hove point. Based on the assumption that this observation also holds in the more complicated situation of an abrupt change in the hopping amplitude [cf. Eq. (26b)], we will thus perform all calculations away from half-filling and simply extrapolate the final results when we discuss the half-filled situation.

To obtain the solution nonperturbatively, we need a closed equation for the sum of all linked clusters. We first split the diagrams into two sets of equivalent diagrams $C(t) = C_{\mathrm{red}}(t) + C_{\mathrm{blue}}(t)$ (Fig. 17), each of which has a vertex of the aforementioned type and generates the other propagator with the swap $V \leftrightarrow \bar{V}$. (One can always do this due to the form of the potential: for every connected diagram there exists a corresponding diagram with the vertices flipped.)

We now take $C_{\mathrm{blue}}(t)$ and isolate the blue vertex. The remaining parts of the propagator then form diagrams for the hopping propagator in the time-dependent potential $V(\tau)$. We can resum these diagrams to obtain the fully normalized electron hopping propagator. The $1/n$ symmetry factor can be taken care of by multiplying each vertex with λ and integrating with respect to λ at the end [$\int_0^1 d\lambda(\lambda V)^n = V^n/n$]. The transient hopping propagator and the transient onsite propagator is given by

$$h_\lambda(\tau) = -i\frac{\langle\mathcal{T}c_{\mathbf{r}_2}(\tau)c^\dagger_{\mathbf{r}_1}(\tau')\exp\{-i\lambda\int dt'\hat{V}(t')\}\rangle}{\langle\mathcal{T}\exp\{-i\lambda\int dt'\hat{V}(t')\}\rangle}, \tag{C3}$$

$$g_\lambda(\tau) = -i\frac{\langle\mathcal{T}c_{\mathbf{r}_1}(\tau)c^\dagger_{\mathbf{r}_1}(\tau')\exp\{-i\lambda\int dt'\hat{V}(t')\}\rangle}{\langle\mathcal{T}\exp\{-i\lambda\int dt'\hat{V}(t')\}\rangle}. \tag{C4}$$

The expression we desire is obtained by reintroducing the removed vertex and integrating the normalized propagator h_λ:

$$C_{\mathrm{blue}}(t) = -V\int_0^t d\tau\int_0^1 d\lambda\, h_\lambda(\tau,\tau+|t). \tag{C5}$$

The two transient propagator Eqs. (C3) and (C4) satisfy the coupled Dyson-Schwinger equations:

$$h_\lambda(\tau,\tau'|t,t') = h_0(\tau-\tau')+\lambda V\int_t^{t'} h_0(\tau-\tau'')h_\lambda(\tau'',\tau'|t,t') + \lambda\bar{V}\int_t^{t'} g_0(\tau-\tau'')g_\lambda(\tau'',\tau'|t,t'), \tag{C6}$$

$$g_\lambda(\tau,\tau'|t,t') = g_0(\tau-\tau')+\lambda V\int_t^{t'} g_0(\tau-\tau'')h_\lambda(\tau'',\tau'|t,t') + \lambda\bar{V}\int_t^{t'} h_0(\tau-\tau'')g_\lambda(\tau'',\tau'|t,t'). \tag{C7}$$

One gets an equal number of corresponding diagrams C_{red} which one can obtain by making the replacement $V \to \bar{V}$ in C_{blue}. This gives us the full propagator

$$C(t) = -V\int_0^t d\tau\int_0^1 d\lambda\, h_\lambda(\tau,\tau+|t) + (V\mapsto\bar{V}). \tag{C8}$$

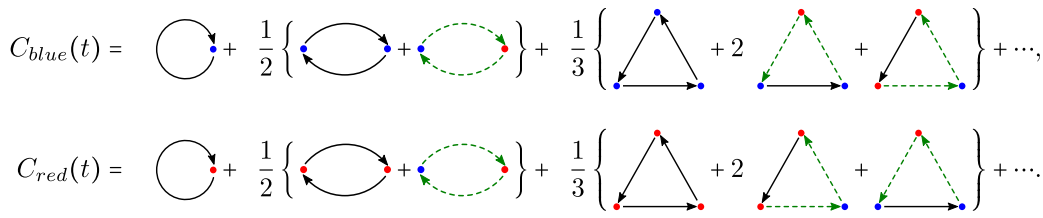

FIG. 17. The pair of equations, $C_{\text{red}}(t)$ and $C_{\text{blue}}(t)$, that sum to give the total propagator $C(t)$ and are related to each other by conjugating the vertices $V \leftrightarrow \bar{V}$.

In the energy representation,

$$g_0(\omega) = \int dE \frac{\rho(E)}{\omega - E + i\delta\,\text{sign}(E)}, \tag{C9}$$

where $\rho(E)$ is the density of states,

$$\rho(E) = \int \frac{d^2k}{(2\pi)^2}\delta(E - \{-2w(\cos k_x + \cos k_y) - \mu\})$$
$$= \frac{1}{4\pi^2 w} K\left\{\left[1 - \left(\frac{E+\mu}{4w}\right)^2\right]^{\frac{1}{2}}\right\}$$

and $K(x)$ is the modified Bessel function. Similarly,

$$h_0(\omega) = \int dE \frac{\rho^h(E)}{\omega - E + i\delta\,\text{sign}(E)} \tag{C10}$$

with the "hopping" density of states ρ^h defined as

$$\rho^h(E) = \int \frac{d^2k}{(2\pi)^2} e^{ik_y}\delta(E - \{-2w(\cos k_x + \cos k_y) - \mu\})$$
$$= -\frac{1}{4w}(E+\mu)\rho(E). \tag{C11}$$

The integral can be evaluated in closed form due to the rotational symmetry of the 0-flux band dispersion. Away from half-filling, the small frequency behavior of the propagators can be approximated as

$$g_0(\omega) \approx A - i\pi\rho(0)\text{sign}(\omega), \tag{C12a}$$
$$h_0(\omega) \approx B - i\pi\rho^h(0)\text{sign}(\omega), \tag{C12b}$$

where A, B are real constants. It is apparent that the long-time behaviors of both propagators are $g_0(t), h_0(t) \sim 1/t$.

To solve for the normalized propagator, we first decouple the Dyson-Schwinger equations. Repressing all arguments except for the first since that is the only one that changes in the calculations,

$$h_\lambda = \frac{-\rho_0^h}{\tau - \tau'} + \lambda \int_0^t d\tau'' \frac{V\rho_0^h h_\lambda(\tau'') + \bar{V}\rho_0 g_\lambda(\tau'')}{\tau'' - \tau}, \tag{C13}$$

$$g_\lambda = \frac{-\rho_0}{\tau - \tau'} + \lambda \int_0^t d\tau'' \frac{V\rho_0 h_\lambda(\tau'') + \bar{V}\rho_0^h g_\lambda(\tau'')}{\tau'' - \tau}. \tag{C14}$$

To decouple these equations, one must compute the left eigenvectors and eigenvalues of the matrix

$$\mathbf{M} = \lambda \begin{pmatrix} V\rho_0^h & \bar{V}\rho_0 \\ V\rho_0 & \bar{V}\rho_0^h \end{pmatrix}. \tag{C15}$$

The eigenvalue equation for $\mathbf{M}$ gives

$$\mu^2 - \lambda\rho_0^h(V + \bar{V})\mu + |\lambda V|^2\left[\left(\rho_0^h\right)^2 - (\rho_0)^2\right] = 0, \tag{C16}$$

$$\mu = \lambda\rho_0^h \Re V \pm \lambda\sqrt{|V|^2(\rho_0)^2 - \left(\text{Im}V\rho_0^h\right)^2} \tag{C17}$$

and the left eigenvector $\mathbf{a} \equiv (1, a)$ is defined by the characteristic equation

$$\lambda V\rho_0^h + a\lambda V\rho_0 = \mu_{1,2} \tag{C18}$$

with the solutions

$$a_{1,2} = \frac{1}{V\rho_0}\left(\mu_{1,2}/\lambda - V\rho_0^h\right). \tag{C19}$$

The decoupled equations are

$$\{h + a_{(1,2)}g\}_\lambda(\tau)$$
$$= -\frac{\rho_0^h + a_{(1,2)}\rho_0}{\tau - \tau'} + \mu_{1,2}\int_0^t d\tau'' \frac{\{h + a_{(1,2)}g\}_\lambda(\tau'')}{\tau'' - \tau}. \tag{C20}$$

This expression simplifies nicely due to Eq. (C18), leaving us with

$$\{h + a_{(1,2)}g\}_\lambda(\tau)$$
$$= -\frac{\mu_{1,2}}{\lambda V(\tau - \tau')} + \mu_{1,2}\int_0^t d\tau'' \frac{\{h + a_{(1,2)}g\}_\lambda(\tau'')}{\tau'' - \tau}. \tag{C21}$$

Using the textbook [94], one can directly read off the solution

$$C_{\text{blue}}(t) = -V\int_0^t d\tau \int_0^1 d\lambda \left(\frac{a_2}{a_2 - a_1}\right)\{h + a_1 g\}_\lambda(\tau, \tau + |t)$$
$$- \left(\frac{a_1}{a_2 - a_1}\right)\{h + a_2 g\}_\lambda(\tau, \tau + |t). \tag{C22}$$

Ignoring the leading-order energy shift, the transient part gives us

$$C_{\text{blue}}(t) = -\left\{\left(\frac{a_2}{a_2 - a_1}\right)\left(\frac{\delta_1}{\pi}\right)^2 + \left(\frac{-a_1}{a_2 - a_1}\right)\left(\frac{\delta_2}{\pi}\right)^2\right\}\ln(t), \tag{C23}$$

where $\delta_i = \arctan(\pi\mu_i/\lambda)$. Now we find C_{red}. Note that while a_i is not invariant under the switch $V \mapsto \bar{V}$, $\mu_{1,2}$ are. This allows for a dramatic cancellation in the full propagator, leaving us with

$$C(t) = -\left\{\left(\frac{\delta_1}{\pi}\right)^2 + \left(\frac{\delta_2}{\pi}\right)^2\right\}\ln(t). \tag{C24}$$

Our final equation will be the above multiplied by N_f to account for internal flavor or spin degrees of freedom, giving Eq. (28).

APPENDIX D: LUTTINGER SURFACE

In this Appendix we present details for the calculation of the Luttinger surface in the orthogonal metal, Sec. VI A 1, starting from Eq. (35) of the main text.

We here use the notation $M_{\mathbf{q}} = \eta h\sqrt{1-2J[\cos(q_x)+\cos(q_y)]} \simeq \eta h(1-\delta M_{\mathbf{q}})$, where $\delta M_{\mathbf{q}} = J[\cos(q_x)+\cos(q_y)]/(\eta h)$. Using the notation

$$G_{\mathrm{OM}}(\mathbf{q},z) = \frac{1}{z-\xi_0(\mathbf{q})-\mathrm{sign}[\xi_0(\mathbf{q})]\eta h} \tag{D1}$$

we thus obtain

$$\begin{aligned}\mathcal{G}(\mathbf{p},z) &= a^2\int_{\mathrm{BZ}}(dq)\frac{\eta h}{M_{\mathbf{q}-\mathbf{p}}}\frac{1}{z-\xi_0(\mathbf{q})-\mathrm{sign}[\xi_0(\mathbf{q})]M_{\mathbf{q}-\mathbf{p}}}\\ &\simeq \underbrace{a^2\int_{\mathrm{BZ}}(dq)G_{\mathrm{OM}}(\mathbf{q},z)}_{\mathcal{G}^{(0)}(z)} + \underbrace{a^2\int_{\mathrm{BZ}}(dq)\delta M_{\mathbf{p}-\mathbf{q}}[G_{\mathrm{OM}}(\mathbf{q},z)-\eta h\,\mathrm{sign}[\xi_0(\mathbf{q})]G_{\mathrm{OM}}(\mathbf{q},z)^2]}_{\mathcal{G}^{(1)}(\mathbf{p},z)}.\end{aligned} \tag{D2}$$

We next use a trigonometric identity to rewrite $\delta M_{\mathbf{p}-\mathbf{q}}$ as a product of functions containing $\mathbf{p}$ and $\mathbf{q}$, exploit that integrals over $\sin(q_{x,y})$ vanish by symmetry, exploit C_4 symmetry, and write

$$\cos(q_x)+\cos(q_y) = -[\xi_0(\mathbf{q})+\mu]/2w, \tag{D3}$$

so that, using $G_{\mathrm{OM}}(\xi,z) = [z-\xi-\mathrm{sign}(\xi)\eta h]^{-1}$,

$$\mathcal{G}^{(0)}(z) = a^2\int d\xi\,\rho(\xi+\mu)G_{\mathrm{OM}}(\xi,z), \tag{D4}$$

$$\begin{aligned}\mathcal{G}^{(1)}(\mathbf{p},z) = \frac{J[\xi_0(\mathbf{p})+\mu]}{8\eta h w^2}a^2\int d\xi\,\rho(\xi+\mu)(\xi+\mu)\\ \times[G_{\mathrm{OM}}(\xi,z)-\eta h\,\mathrm{sign}(\xi)G_{\mathrm{OM}}(\xi,z)^2].\end{aligned} \tag{D5}$$

We next define the following dimensionless integrals

$$I_n^{\pm} = \int_0^{\infty} d\bar{\xi}\frac{\bar{\xi}^{n-1}}{\nu_0}\frac{\rho(\eta h\bar{\xi}+\mu)\pm\rho(\eta h\bar{\xi}-\mu)}{(z/\eta h)^2-(\bar{\xi}+1)^2}, \tag{D6}$$

where $\nu_0 = 1/(2\pi w a^2)$ and

$$\rho(\xi) = \nu_0\theta[(2w)^2-\xi^2]\frac{4wK[1-(2w/\xi)^2]}{\pi|\xi|} \tag{D7}$$

is the particle-hole-symmetric density of states of the square lattice centered around zero and $K(x)$ denotes a Bessel function of the second kind.

Using this notation we find

$$\mathcal{G}^{(0)}(z) = \frac{z}{\eta h}a^2\nu_0 I_1^+ + a^2\nu_0(I_1^- + I_2^-), \tag{D8}$$

$$\begin{aligned}\mathcal{G}^{(1)}(\mathbf{p},z) = [\xi_0(\mathbf{p})+\mu]\frac{J}{8w^2}a^2\nu_0\Big\{I_2^+ + I_3^+ + \eta h\partial_z\\ \times(I_2^- + I_3^-) + \frac{\mu}{\eta h}[I_1^- + I_2^- + \eta h\partial_z(I_1^+ + I_2^+)]\\ + \frac{z}{\eta h}I_2^- + \partial_z(zI_2^+) + \frac{\mu z}{(\eta h)^2}I_1^+ + \frac{\mu}{\eta h}\partial_z(zI_1^-)\Big\}.\end{aligned} \tag{D9}$$

We concentrate on the vicinity of half-filling, i.e., $\mu = 0$. We thus assume also z to be small and drop all orders $z^2, \mu^2, z\mu, zJ$, etc. In this limit, we only need the following combination of integrals (in addition to $I_1^+ < 0$):

$$2I_2^+ + I_3^+ \simeq -I_1^+ - \frac{2}{\nu_0\eta h} < 0, \tag{D10}$$

$$I_1^- + I_2^- \simeq \frac{1}{\nu_0\eta h}[n(\mu)-n(-\mu)], \tag{D11}$$

where $n(\mu)$ is the fractional filling

$$n(\mu) = \int_{-\infty}^{0} d\xi\,\rho(\xi+\mu). \tag{D12}$$

This leads to

$$\mathcal{G}^{(0)}(z) = \frac{a^2\nu_0}{\eta h}\left(zI_1^+ + \frac{1}{\nu_0}[n(\mu)-n(-\mu)]\right), \tag{D13}$$

$$\mathcal{G}^{(1)}(\mathbf{p},z) = -[\xi_0(\mathbf{p})+\mu]\frac{J}{8w^2}a^2\nu_0\left(I_1^+ + \frac{2\pi w}{\eta h}\right), \tag{D14}$$

which can be rewritten as

$$\begin{aligned}\mathcal{G}(\mathbf{p},z) &\simeq a^2\frac{\nu_0 I_1^+}{\eta h}\left[z + \frac{1}{\nu_0}\frac{n(\mu)-n(-\mu)}{I_1^+}\right.\\ &\quad\left. + \frac{J\eta h}{4w}\frac{I_1^+ + 2\pi w/\eta h}{I_1^+}\sum_{\mu=x,y}\cos(q_\mu)\right]\end{aligned} \tag{D15}$$

$$=: -\frac{1}{\mathcal{Z}}[z+\zeta_0(\mathbf{p})], \tag{D16}$$

which is the result quoted in Eq. (36) of the main text.

APPENDIX E: CRITICALITY OF ELECTRIC STRINGS IN THE OM PHASE

In this Appendix we derive Eq. (37). Both coefficients λ and λ_0 arise from the self-interaction of the critical electric strings. The four-point correlation function corresponding to λ_0 arises from vertices with 2 e particles and 2 e antiparticles interacting. Since we only require the connected part to calculate the nonlinearity, we must subtract from Eq. (23) the pairwise distinct interaction of e-particle and -antiparticle

pairs, i.e., noninteracting electric strings,

$$V_0(\{\mathbf{r},\tau\}) = J^4 \prod_{n=1}^{4} \sum_{\mathbf{r}} \delta_{\langle \mathbf{r}_n,\mathbf{r}\rangle} \times \left[\exp\left\{ h \sum_{i=1}^{n} \tau_{p(i)} \mathrm{Re}\left[\omega^{-\sum_{j=1}^{i} q_{p(j)}} (1-\omega^{q_{p(i)}})\right]\right\} - D(\tau_1,\tau_2)D(\tau_3,\tau_4) - D(\tau_1,\tau_3)D(\tau_2,\tau_4) - D(\tau_1,\tau_4)D(\tau_2,\tau_3)\right]. \tag{E1}$$

Except for the special case $N=2$, one of the three terms in the pairwise interactions always evaluates to 0 due to Feynman rule 2. To find the vertex for the continuum field theory, we evaluate Eq. (E1) at zero frequency, taking $\beta \equiv 1/T$ as the infrared cutoff for the theory

$$\begin{aligned}
&\int_0^\beta \prod_{n=1}^{N} (d\tau_n)\, V_0(\{\mathbf{r},\tau\}) \\
&= J^4 \sum_{\mathbf{r}} \delta_{\langle \mathbf{r}_i,\mathbf{r}\rangle} \left[16\left(\frac{3}{(\eta h)^4} - \frac{2\beta}{(\eta h)^3} + \frac{\beta^2}{2(\eta h)^2}\right) \right. \\
&\quad \left. + \frac{8}{(\eta-2)^2}\left(\frac{4\eta-9}{(\eta h)^2} - \beta \frac{2-\eta}{2(\eta h)^3}\right)\right] \\
&\quad - 2\frac{4J^4}{h^2\eta^2}\left(\beta - \frac{1}{\eta h}\right)^2 \\
&\overset{O(\beta)}{=} -\beta \frac{J^4}{(\eta h)^3}\left(16 + \frac{4}{\eta-2}\right) \sum_{\mathbf{r}} \delta_{\langle \mathbf{r}_i,\mathbf{r}\rangle}.
\end{aligned} \tag{E2}$$

The $\mathbb{Z}_N$ vertex has two terms, each of which corresponds to the creation (ϕ^N) and annihilation ($\bar{\phi}^N$) of N e particles, respectively. Unlike the 4-vertex, there are no lower-order contributions that need to be subtracted from the connected part of the propagator. Since all charges are 1 (for the creation term, -1 for the annihilation term), Eq. (23) can be simplified to

$$V(\{\mathbf{r},\tau\}) = J^N \prod_{n=1}^{N} \sum_{\mathbf{r}} \delta_{\langle \mathbf{r}_n,\mathbf{r}\rangle} \exp\left\{ h \sum_{=1}^{N} \tau_{p(i)} \mathrm{Re}[\omega^{-i}(1-\omega)]\right\}. \tag{E3}$$

The corresponding imaginary-time integral with the IR cutoff at β has no closed form in terms of N, but dimensionally, one can observe that the exponent is of the order of J^N/h^{N-1}.

The addition of the nearest-neighbor hopping perturbation t introduces new operators that in the critical limit give rise to interactions between strings and fermionic excitations, captured by the action $\mathcal{S}_{\mathrm{IA}}$. The interaction (local in time) takes the form

$$V\left(\mathbf{r}_c, \mathbf{r}_{c^\dagger}; \mathbf{r}_{D_1}, \mathbf{r}_{\bar{D}_2}\right) = t\, \delta_{\mathbf{r}_c,\mathbf{r}_{D_1}} \delta_{\mathbf{r}_{c^\dagger},\mathbf{r}_{\bar{D}_2}} \delta_{\langle \mathbf{r}_{c^\dagger},\mathbf{r}_c\rangle}. \tag{E4}$$

Upon rescaling the fields, we arrive at the coupling constant $\gamma \sim \eta h t a^2[\cos(k_x) + \cos(k_y)]$ in the long-wavelength limit of the ϕ fields.

APPENDIX F: HADRON FORMATION IN LARGE-$K\eta/g$ LIMIT: LADDER RESUMMATION

In this Appendix, we present details on the formation of hadrons. We concentrate on the large-$K\eta/g$ limit, in which we calculate the temperature at which N-particle propagators form bound states.

We now evaluate the N-particle Green's function (see Fig. 12) and consider first the noninteracting limit:

$$\begin{aligned}
\mathbb{L}(\mathbf{q}, i\nu) &= T^{N-1} \prod_{i=1}^{N} \left[\int (d\mathbf{p}_i) \sum_{\epsilon_i} \frac{1}{i\epsilon_i - \xi(\mathbf{p}_i)} \right. \\
&\quad \left. \times \delta\left(\sum \mathbf{p}_i - \mathbf{q}\right) \delta_{(\sum \epsilon_i),\nu}\right] \\
&= \int \prod_{i=1}^{N} (d\mathbf{p}_i) \int_0^\beta d\tau\, e^{-i\nu\tau} \delta^{(2)}\left(\sum \mathbf{p}_i - \mathbf{q}\right) \\
&\quad \times \left(T \sum_{\epsilon_i} \frac{e^{i\epsilon_i\tau}}{i\epsilon_i - \xi(\mathbf{p}_i)}\right).
\end{aligned} \tag{F1}$$

In the second step, we have used the identity $\int_0^\beta (d\tau) e^{i\omega_n\tau} = \beta\delta_{\omega_n,0}$ for a bosonic Matsubara frequency ω_n. This necessitates that the Matsubara frequency ν is bosonic when N is even and fermionic when N is odd, capturing the statistic of the composite excitation. To calculate the sum over fermionic Matsubara frequencies ϵ_i, we employ the usual contour integration

$$\begin{aligned}
T \sum_{\epsilon_i} \frac{e^{i\epsilon_i\tau}}{i\epsilon_i - \xi(\mathbf{p}_i)} &= -\frac{1}{2\pi i} \oint dz\, \frac{e^{z\tau}}{z-\xi} \times \frac{1}{e^{\beta z}+1} \\
&= n_{\mathrm{f}}(\xi) e^{\xi\tau}.
\end{aligned} \tag{F2}$$

The integral becomes

$$\begin{aligned}
\mathbb{L} &= \int_0^\beta d\tau \int \prod_i (dp_i)\, e^{-i\nu\tau} (n_{\mathrm{f}}(\xi_i) e^{\xi_i\tau}) \delta^{(2)}\left(\sum_i \mathbf{p}_i - \mathbf{q}\right) \\
&= \int \prod_i (dp_i)\, \delta^{(2)}\left(\sum_i \mathbf{p}_i - \mathbf{q}\right) n_f(\xi_i) \frac{e^{-i\nu\beta} e^{\sum_i \xi_i} - 1}{\sum_i \xi_i - i\nu}.
\end{aligned} \tag{F3}$$

For now, we assume even N. One would like to examine the behavior of this ladder propagator at $\mathbb{L}(\mathbf{q}=0, i\nu=0)$; $\mathbb{L}_0$. For $N=2$, one recovers the standard result for the Cooper instability in a Fermi liquid. For a general N, the propagator can be rewritten as

$$\mathbb{L}_0 = \int \prod_i (d\mathbf{p}_i)\, \delta^{(2)}\left(\sum_i \mathbf{p}_i\right) \left[\prod_i n_f(-\xi_i) - \prod_i n_f(\xi_i)\right]. \tag{F4}$$

The term in square brackets is nonzero only when all excitations are electrons ($\xi > 0$) or holes ($\xi < 0$). In the limit of low filling, we can assume a parabolic (and thereby radially symmetric) dispersion relation [$p_i = \sqrt{2m(\mu + \xi_i)}$]. One then replaces the momentum-conserving Dirac delta by averaging

it out over the N momenta

$$\left\langle \delta^{(2)}\left(\sum_i \mathbf{p}_i\right)\right\rangle = 2\pi \int dr\, r\left(\prod_i J_0(p_i r)\right). \tag{F5}$$

Performing a change of variables $\mathbf{p}_i \to \xi_i, d\mathbf{p}_i \to \rho d\xi_i$, where ρ is the density of states,

$$\mathbb{L}_0 = \rho^N \int_{-\mu} \prod_i d\xi_i \int dr(2\pi r) \frac{\prod_i J_0[p_i(\xi_i)r]}{\sum_i \xi_i} \times \left[\prod_i n_f(-\xi_i) - \prod_i n_f(\xi_i)\right]. \tag{F6}$$

If the effective interaction between the fermions occurs in a range of energies around the Fermi surface: $\xi_i \in [-\omega_0, \omega_0]$ and $\omega_0 \ll \mu$, the integral over the Bessel functions can be estimated by setting the momentum as the Fermi momentum

$$2\pi \int r\, dr\, [J_0(p_f r)]^N = \frac{4\pi}{p_f^2} c_N. \tag{F7}$$

While c_2 diverges (this is a manifestation of the Cooper logarithm), c_N with $N \geqslant 3$ are all finite and fall off asymptotically as $1/N$ for large N. We highlight that the assumption of a retarded interaction $\omega_0 \ll \mu$ is not valid in the case of g perturbations, instead all states up to the band edge are involved $\omega_0 \sim \mu$. Therefore, while our calculations can be expected to be parametrically correct, nonuniversal constants from ultraviolet processes may be missed.

At finite temperature, approximating the Fermi distribution function as a cutoff to the integral, one gets

$$\mathbb{L}_0 \simeq -2\frac{\rho^N}{p_f^2} 4\pi c_N \underbrace{\int_T^{\omega_0} \prod_i d\xi_i \frac{1}{\sum_i \xi_i}}_{\omega_0^{N-1}\alpha_N(T/\omega_0)}. \tag{F8}$$

For small T, the integral can be further approximated by a Taylor expansion to first order about 0: $\alpha_N(T/\omega_0) \approx \alpha_N(0) - N\frac{T}{\omega_0}\alpha_{N-1}(0)$.

We expect that the fermions have an attractive interaction induced due to H_g whose strength is $\mathcal{V}$. The effective interaction vertex in the N-particle channel $\mathcal{V}_{\text{eff}}$ is therefore

$$\mathcal{V}_{\text{eff}} = \frac{\mathcal{V}}{1 - \mathcal{V}\mathbb{L}_0}. \tag{F9}$$

The onset of hadron instability is characterized by the development of a singularity in the vertex, which occurs when

$$\mathbb{L}_0 = \mathcal{V}^{-1}. \tag{F10}$$

Defining the scaled interaction v as

$$v = -2\mathcal{V}\frac{\rho^N}{p_F^2} 4\pi c_N \omega_0^{N-1} \tag{F11}$$

(see Fig. 13), the critical temperature T_h where Eq. (F10) holds is

$$T_h = \underbrace{\frac{\omega_0 \alpha_N(0)}{N\alpha_{N-1}(0)}}_{T_h^{(0)}} \left(1 - \frac{1}{v\alpha_N(0)}\right). \tag{F12}$$

For odd N, the ladder propagator must be evaluated at $\nu = \pm\pi\beta$, the minimum fermionic Matsubara frequency. This changes the integrand in Eq. (F8) to $[\sum_i \xi_i + (\pi T)^2/(\sum_i \xi_i)]^{-1}$. Up to first order in T, this change does not significantly alter the integral and one can safely proceed with the result for even N.

As mentioned in the main text, the bare interaction $\mathcal{V}$ is expected to scale as $(wg)^N/(\Delta E)^{2N-1}$. By substituting into Eq. (F11) and assuming low filling, one can show that in terms of w, g and the filling μ' (above zero filling), v scales as

$$v \sim \left(\frac{g}{\Delta E_m}\right)^N \left(\frac{w}{\Delta E_m}\right)\left(\frac{\mu}{\Delta E_m}\right)^{N-2}. \tag{F13}$$

APPENDIX G: CONNECTION TO QED$_3$

This Appendix is devoted to making a connection between our $\mathbb{Z}_N$ model and QED$_3$. We first discuss the limit $N \to \infty$ of our model, in order to identify the coupling constants of both theories. Next, starting from a deconfining state of QED$_3$ in the presence of a Fermi surface, we study the RG relevance of $\mathbb{Z}_N$ perturbations and thereby provide technical details for Sec. VII of the main text.

1. $\mathbb{Z}_N$ to QED$_3$

In this Appendix we present the connection between the Hamiltonians of $\mathbb{Z}_N$ and U(1) gauge theories in the limit of large h. Concentrating on the limit $\phi = 0$ the gauge theory part of our model is

$$\mathcal{H} = -\frac{g}{2}\sum_{\mathbf{r}}\sum_{\hat{e}\in\{x,y\}}(\tau_{\mathbf{r},\hat{e}} + \tau^\dagger_{\mathbf{r},\hat{e}}) - \frac{K}{2}\sum_{\mathbf{p}}(B_{\mathbf{p}} + B^\dagger_{\mathbf{p}}). \tag{G1}$$

We now consider the limit $N \to \infty$ and make connection to a compact QED$_3$ with gauge potential $a_{\mathbf{r},\hat{e}}$ on each link. Note the slight difference in notation to the main text, in which $\mathbf{b}$ denotes a link, rather than the multi-index $(\mathbf{r}, \hat{e})$. This is to facilitate the interpretation as a line integral over the U(1) potential. By imposing the same algebra as Eq. (3) we can identify

$$\tau_{\mathbf{r},\hat{e}} + \tau^\dagger_{\mathbf{r},\hat{e}} = \cos\left(\frac{2\pi}{N} i\frac{\partial}{\partial a_{\mathbf{r},\hat{e}}}\right), \tag{G2}$$

$$B_{\mathbf{p}} + B^\dagger_{\mathbf{p}} = 2\cos(\Phi_{\mathbf{p}}), \tag{G3}$$

where $\Phi_{\mathbf{p}}$ is the flux passing through the plaquette $\mathbf{p}$, i.e., the directed sum of vector potentials $a_{\mathbf{r},\hat{e}}$ defined on each link. Thus, the Hamiltonian becomes

$$H = -g\sum_{\mathbf{r}}\sum_{\hat{e}\in\{x,y\}}\cos\left(\frac{2\pi}{N} i\frac{\partial}{\partial a_{\mathbf{r},\hat{e}}}\right) - K\sum_{\mathbf{p}}\cos(\Phi_{\mathbf{p}}). \tag{G4}$$

The first term contains the conjugate "electric" field $E_{\mathbf{r},\hat{e}} \equiv i\frac{\partial}{\partial a_{\mathbf{r},\hat{e}}}$ endowed with the commutation relation $[E_{\mathbf{r},\hat{e}}, a_{\mathbf{r}',\hat{e}'}] = i\delta_{\mathbf{r},\mathbf{r}'}\delta_{\hat{e},\hat{e}'}$. We carefully take the continuum limit and expand the Hamiltonian about its minima. After sorting out the factors of the lattice constant inside the vector potential, we obtain the Hamiltonian

$$H = \int d^2x \frac{g}{2}\left(\frac{2\pi}{N}\right)^2 (E_x^2 + E_y^2) + \frac{Ka^2}{2}B^2. \tag{G5}$$

Given this Hamiltonian, the corresponding QED_3 action is

$$S = \int dt\, d^2x \left[\frac{N^2}{2g(2\pi)^2}\dot{A}^2 - \frac{Ka^2}{2}(\nabla \times A)^2\right], \tag{G6}$$

$$S = \frac{Ka^2}{2}\int dt\, d^2x \sum_{\mu=1}^{3} A_\mu\left(\frac{N^2}{gK(2\pi a)^2}\partial_t^2 - \nabla^2\right)A_\mu, \tag{G7}$$

with the speed of light $c = \sqrt{gK}(2\pi a/N)$. The fermionic part of the Hamiltonian is coupled to this $\mathbb{Z}_N$ gauge field as

$$\mathcal{H}_f = -w\sum_{\mathbf{r}}\sum_{\hat{e}\in\{x,y\}} c^\dagger_{\mathbf{r}} e^{-ia_{\mathbf{r},\hat{e}}} c_{\mathbf{r}+\hat{e}} + \text{H.c.} \tag{G8}$$

This corresponds to a Peierls substitution where the line integral of the U(1) gauge potential $[a_{\mathbf{r},\hat{e}} = \int_{\mathbf{r}}^{\mathbf{r}+\hat{e}} A(\mathbf{r}')\cdot d\mathbf{r}']$ modifies the hopping between sites. Taking the continuum limit recovers the Hamiltonian of fermions coupled to a U(1) gauge field

$$\mathcal{H}_w = \frac{wa^2}{2}\int d^2x\, \psi^\dagger_{\mathbf{x}}(-i\nabla - A)^2\psi_{\mathbf{x}}. \tag{G9}$$

2. RG flow calculations for $\mathbb{Z}_N$ perturbation in QED_3

We now determine the regime in which the $\mathbb{Z}_N$ physics dominates the QED_3 action. Namely, we ask when is the action

$$S = \int d\tau\, d^2x \sum_{\mu=1}^{3} A_\mu\left[-\nabla^2 - \partial_\tau^2\right]A_\mu + S_{\text{fermions}} \tag{G10}$$

stable to the $\mathbb{Z}_N$ perturbation

$$\delta S = \int d\tau\, d^2x\, \lambda[\cos(NA_x) + \cos(NA_y)]. \tag{G11}$$

We work in the Coulomb gauge ($\nabla\cdot\mathbf{A} = 0$), where the propagator takes the form [37]

$$\mathbb{D}_T[Q \equiv (\nu, \mathbf{q})] = \frac{1}{\gamma\frac{|\nu|}{q} + q^2\chi_D}, \tag{G12}$$

where on the bare level $\gamma \sim N_f k_F$ and $\chi_D \sim N_f/m$.

Formally, this propagator is obtained by introducing N_f flavors of fermions followed by a large-N_f (and [39] an ϵ) expansion. The action takes the form

$$S_T = \int \frac{d\nu\, d^2\mathbf{q}}{(2\pi)^3}|A_T(Q)|^2\left[\gamma\frac{|\nu|}{q} + q^2\chi_D\right]\Big/a^2. \tag{G13}$$

Here, $A_T(Q)$ is the transverse part of the gauge-fixed vector potential $[\mathbf{A}(Q) = A_T(Q)[\hat{z}\times\mathbf{q}]]$ and a is the lattice spacing. Our RG procedure now splits the phase space into two parts, the slow and fast fluctuations:

$$\sqrt{(\gamma\nu)^2 + (\chi_D q^3)^2} \in \left[0, \frac{\Lambda}{b_\nu}\right] \quad \text{(slow)}, \tag{G14}$$

$$\sqrt{(\gamma\nu)^2 + (\chi_D q^3)^2} \in \left(\frac{\Lambda}{b_\nu}, \Lambda\right] \quad \text{(fast)}, \tag{G15}$$

where Λ is the UV cutoff. The quadratic action decouples in the slow and fast fluctuations. We discard the fast fluctuations and rescale the remaining action

$$\nu' \to b_\nu\nu, \quad \mathbf{q}' \to b\mathbf{q}. \tag{G16}$$

One can immediately see that for the propagator to retain its standard form $b_\nu = b^3$, which motivated the choice for the momentum shells. Assuming that the U(1) gauge field scales as

$$\left|A_T^<\left(\frac{\nu}{b^3}, \frac{\mathbf{q}}{b}\right)\right| = b^5|A_T(\nu,\mathbf{q})|, \tag{G17}$$

the action thus scales as

$$S_T^< = b^3\int_{[0,\Lambda]}\frac{d\nu\, d^2\mathbf{q}}{(2\pi)^3}|A_T(Q)|^2\left[\gamma\frac{|\nu|}{q} + q^2\chi_D\right]\Big/a^2. \tag{G18}$$

Under this momentum-shell RG procedure, the $\mathbb{Z}_N$ perturbation scaling is

$$\delta S^< = -\lambda\int d\tau\, d^2\mathbf{x}\sum_{i=\{x,y\}}\frac{1}{2}\langle e^{iN(A_i^> + A_i^<)} + e^{-iN(A_i^> + A_i^<)}\rangle_>$$

$$= -\lambda\int d\tau\, d^2\mathbf{x}\sum_{i=\{x,y\}}\cos(NA_i^<)e^{-\frac{N^2}{2}\langle(A_i^>)^2\rangle}, \tag{G19}$$

$$\langle(A_i^>)^2\rangle = \frac{1}{(2\pi)^3}\int_{\text{fast}} d\nu\, d^2\mathbf{q}\, a^2\frac{[\hat{z}\times\mathbf{q}]_i^2}{\gamma\frac{|\nu|}{q} + \chi_D q^2}$$

$$= \frac{a^2}{2(2\pi)^3}\int_{\text{fast}} d\nu\, d^2\mathbf{q}\,\frac{1}{\gamma\frac{|\nu|}{q} + \chi_D q^2}$$

$$= \frac{a^2}{(2\pi)^3}\int_{\text{fast},\,\nu>0} d\nu\, d^2\mathbf{q}\,\frac{1}{\gamma\frac{\nu}{q} + \chi_D q^2}. \tag{G20}$$

Switching to polar coordinates and making the substitution

$$\bar{\nu} = \gamma\nu, \quad \bar{q} = (\chi_D)^{1/3}q, \tag{G21}$$

the integral is simplified to

$$\langle(A_i^>)^2\rangle = \frac{a^2}{(2\pi)^2}\frac{1}{\gamma\chi_D}\int_{\text{fast},\bar{\nu},\bar{q}>0} d\bar{\nu}\, d\bar{q}\,\frac{\bar{q}^2}{\bar{\nu} + \bar{q}^3}$$

$$= \frac{a^2}{12\pi^2}\frac{1}{\gamma\chi_D}\int_{\substack{\bar{\nu},\bar{x}>0\\ \sqrt{\bar{\nu}^2+\bar{x}^2}\in(\Lambda/b^3,\Lambda]}} d\bar{\nu}\, d\bar{x}\,\frac{1}{\bar{\nu} + \bar{x}}, \tag{G22}$$

where $\bar{x} = \bar{q}^3$. Making another polar transformation [$\bar{\nu} = r\sin(\theta), \bar{x} = r\cos(\theta)$],

$$\langle(A_i^>)^2\rangle = \frac{a^2}{12\pi^2}\frac{1}{\gamma\chi_D}\int_{\Lambda/b^3}^{\Lambda} dr\int_0^{\frac{\pi}{2}}\frac{d\theta}{\sin(\theta) + \cos(\theta)}$$

$$= \frac{\tilde{\Lambda}}{\chi_D\gamma}(1 - b^{-3}), \tag{G23}$$

where $\tilde{\Lambda} \propto \Lambda$ is a velocity corresponding to the UV cutoff and has hence the same dimensions as $\gamma\chi_D$.

From Eq. (G23), the $\mathbb{Z}_N$ perturbation scales as

$$\delta S^< = -\lambda\exp\left\{\frac{N^2}{2}\frac{\tilde{\Lambda}}{\chi_D\gamma}(1 - b^{-3})\right\}$$

$$\times\int d\tau\, d^2\mathbf{x}\sum_{i=\{x,y\}}\cos(NA_i^<). \tag{G24}$$

Examining Eq. (G24), λ scales under the RG procedure as

$$\lambda \to b^5\exp\left\{-\frac{N^2}{\tilde{\chi}\tilde{\gamma}}(1 - b^{-3})\right\}\lambda, \tag{G25}$$

where the cutoff has been absorbed into a redefinition of couplings denoted $\tilde{\chi}$ and $\tilde{\gamma}$. The tree-level RG flow equations are

$$\frac{d\tilde{\chi}}{d\ \ln b} = 3\tilde{\chi}, \tag{G26}$$

$$\frac{d\tilde{\gamma}}{d\ \ln b} = 3\tilde{\gamma}, \tag{G27}$$

$$\frac{d\lambda}{d\ \ln b} = \left(5 - 3\frac{N^2}{\tilde{\chi}\tilde{\gamma}}\right)\lambda. \tag{G28}$$

Introducing the dimensionless coupling $\kappa = \tilde{\gamma}\tilde{\chi} \overset{\text{bare value}}{=} N_f^2 v_F/\tilde{\Lambda}$, we obtain the RG equations presented in Eq. (44) of the main text. One can see that for however large N, since κ is a relevant parameter under RG scaling, the $\mathbb{Z}_N$ parameter λ always becomes relevant. Thus, there is no U(1) phase in the system.

We can, however, estimate the regime in which the system approximately behaves as QED_3. From the tree-level flow Eqs. (G26) and (G27),

$$\frac{d\kappa}{d\ \ln(L/l)} = 6\kappa \Rightarrow \kappa = \kappa_0\left(\frac{L}{l}\right)^6. \tag{G29}$$

The $\mathbb{Z}_N$ perturbation scaling λ does not grow as long as $\kappa = \frac{3N^2}{5}$. This endows a critical size to the system $L_{\text{crit}} = l(\frac{3N^2}{5\kappa_0})^{1/6}$. For $L < L_{\text{crit}}$, a U(1) phase can be well approximated. It is natural to assume $\tilde{\Lambda} \sim v_F$, so that the bare $\kappa = N_f^2$ (up to a coefficient of order one) and to set $l = 1/k_F$.

[1] Franz J Wegner, Duality in generalized Ising models and phase transitions without local order parameters, J. Math. Phys. **12**, 2259 (1971).

[2] Kenneth G. Wilson, Confinement of quarks, Phys. Rev. D **10**, 2445 (1974).

[3] John B. Kogut, An introduction to lattice gauge theory and spin systems, Rev. Mod. Phys. **51**, 659 (1979).

[4] Raúl A. Briceño, Jozef J. Dudek, and Ross D. Young, Scattering processes and resonances from lattice QCD, Rev. Mod. Phys. **90**, 025001 (2018).

[5] Subir Sachdev, Topological order, emergent gauge fields, and Fermi surface reconstruction, Rep. Prog. Phys. **82**, 014001 (2019).

[6] Lucile Savary and Leon Balents, Quantum spin liquids: A review, Rep. Prog. Phys. **80**, 016502 (2017).

[7] Xiao-Gang Wen, Topological orders in rigid states, Int. J. Mod. Phys. B **04**, 239 (1990).

[8] A Yu Kitaev, Fault-tolerant quantum computation by anyons, Ann. Phys. **303**, 2 (2003).

[9] Emilio Cobanera, Jascha Ulrich, and Fabian Hassler, Changing anyonic ground degeneracy with engineered gauge fields, Phys. Rev. B **94**, 125434 (2016).

[10] Erez Zohar, Alessandro Farace, Benni Reznik, and J. Ignacio Cirac, Digital lattice gauge theories, Phys. Rev. A **95**, 023604 (2017).

[11] Erez Zohar, Alessandro Farace, Benni Reznik, and J. Ignacio Cirac, Digital quantum simulation of $\mathbb{Z}_2$ lattice gauge theories with dynamical fermionic matter, Phys. Rev. Lett. **118**, 070501 (2017).

[12] Patrick Emonts, Mari Carmen Bañuls, Ignacio Cirac, and Erez Zohar, Variational Monte Carlo simulation with tensor networks of a pure $\mathbb{Z}_3$ gauge theory in $(2+1)$D, Phys. Rev. D **102**, 074501 (2020).

[13] Lorenzo Cardarelli, Sebastian Greschner, and Luis Santos, Deconfining disordered phase in two-dimensional quantum link models, Phys. Rev. Lett. **124**, 123601 (2020).

[14] Daniel Robaina, Mari Carmen Bañuls, and J. Ignacio Cirac, Simulating $2+1DZ_3$ lattice gauge theory with an infinite projected entangled-pair state, Phys. Rev. Lett. **126**, 050401 (2021).

[15] Erez Zohar, J Ignacio Cirac, and Benni Reznik, Quantum simulations of lattice gauge theories using ultracold atoms in optical lattices, Rep. Prog. Phys. **79**, 014401 (2016).

[16] Elisa Ercolessi, Paolo Facchi, Giuseppe Magnifico, Saverio Pascazio, and Francesco V. Pepe, Phase transitions in Z_n gauge models: Towards quantum simulations of the Schwinger-Weyl QED, Phys. Rev. D **98**, 074503 (2018).

[17] Alessio Celi, Benoît Vermersch, Oscar Viyuela, Hannes Pichler, Mikhail D. Lukin, and Peter Zoller, Emerging two-dimensional gauge theories in Rydberg configurable arrays, Phys. Rev. X **10**, 021057 (2020).

[18] Simone Notarnicola, Mario Collura, and Simone Montangero, Real-time-dynamics quantum simulation of $(1+1)$-dimensional lattice QED with Rydberg atoms, Phys. Rev. Res. **2**, 013288 (2020).

[19] Ruben Verresen, Mikhail D. Lukin, and Ashvin Vishwanath, Prediction of toric code topological order from Rydberg blockade, Phys. Rev. X **11**, 031005 (2021).

[20] Giacomo Giudice, Federica Maria Surace, Hannes Pichler, and Giuliano Giudici, Trimer states with $\mathbb{Z}_3$ topological order in Rydberg atom arrays, Phys. Rev. B **106**, 195155 (2022).

[21] M. Dalmonte and S. Montangero, Lattice gauge theory simulations in the quantum information era, Contemp. Phys. **57**, 388 (2016).

[22] Mari Carmen Banuls, Rainer Blatt, Jacopo Catani, Alessio Celi, Juan Ignacio Cirac, Marcello Dalmonte, Leonardo Fallani, Karl Jansen, Maciej Lewenstein, Simone Montangero *et al.*, Simulating lattice gauge theories within quantum technologies, Eur. Phys. J. D **74**, 165 (2020).

[23] KJ Satzinger, Y-J Liu, A Smith, C Knapp, M Newman, C Jones, Z Chen, C Quintana, X Mi, A Dunsworth *et al.*, Realizing topologically ordered states on a quantum processor, Science **374**, 1237 (2021).

[24] Robert D. Pisarski, Remarks on nuclear matter: How an ω_0 condensate can spike the speed of sound, and a model of $Z(3)$ baryons, Phys. Rev. D **103**, L071504 (2021).

[25] Snir Gazit, Mohit Randeria, and Ashvin Vishwanath, Emergent Dirac fermions and broken symmetries in confined and deconfined phases of Z_2 gauge theories, Nat. Phys. **13**, 484 (2017).

[26] Snir Gazit, Fakher F Assaad, Subir Sachdev, Ashvin Vishwanath, and Chong Wang, Confinement transition of Z_2 gauge theories coupled to massless fermions: Emergent quantum chromodynamics and SO(5) symmetry, Proc. Natl. Acad. Sci. USA **115**, E6987 (2018).

[27] Jan F Haase, Luca Dellantonio, Alessio Celi, Danny Paulson, Angus Kan, Karl Jansen, and Christine A Muschik, A resource efficient approach for quantum and classical simulations of gauge theories in particle physics, Quantum **5**, 393 (2021).

[28] Martin B Einhorn, Robert Savit, and Eliezer Rabinovici, A physical picture for the phase transitions in Z_N symmetric models, Nucl. Phys. B **170**, 16 (1980).

[29] Elahe Samimi, Mohammad Hossein Zarei, and Afshin Montakhab, Conditional global entanglement in a kosterlitz-thouless quantum phase transition, Phys. Rev. A **107**, 052412 (2023).

[30] Mohammad Hossein Zarei, Kosterlitz-thouless phase and Z_d topological quantum phase, Phys. Rev. B **101**, 235126 (2020).

[31] Jorge V. José, Leo P. Kadanoff, Scott Kirkpatrick, and David R. Nelson, Renormalization, vortices, and symmetry-breaking perturbations in the two-dimensional planar model, Phys. Rev. B **16**, 1217 (1977).

[32] Pranay Patil, Hui Shao, and Anders W. Sandvik, Unconventional U(1) to Z_q crossover in quantum and classical q-state clock models, Phys. Rev. B **103**, 054418 (2021).

[33] The case $N = 3$ is special: Here a first-order transition generally occurs, as can be easily seen by considering a complex $|\phi|^4$ theory perturbed by the $\mathbb{Z}_3$-symmetric potential $\phi^3 + \phi^{*3}$.

[34] B. L. Altshuler, L. B. Ioffe, and A. J. Millis, Low-energy properties of fermions with singular interactions, Phys. Rev. B **50**, 14048 (1994).

[35] Yong Baek Kim, Akira Furusaki, Xiao-Gang Wen, and Patrick A. Lee, Gauge-invariant response functions of fermions coupled to a gauge field, Phys. Rev. B **50**, 17917 (1994).

[36] Michael Hermele, T. Senthil, Matthew P. A. Fisher, Patrick A. Lee, Naoto Nagaosa, and Xiao-Gang Wen, Stability of $U(1)$ spin liquids in two dimensions, Phys. Rev. B **70**, 214437 (2004).

[37] Cody P. Nave, Sung-Sik Lee, and Patrick A. Lee, Susceptibility of a spinon Fermi surface coupled to a $U(1)$ gauge field, Phys. Rev. B **76**, 165104 (2007).

[38] Sung-Sik Lee, Low-energy effective theory of Fermi surface coupled with $U(1)$ gauge field in $2 + 1$ dimensions, Phys. Rev. B **80**, 165102 (2009).

[39] David F. Mross, John McGreevy, Hong Liu, and T. Senthil, Controlled expansion for certain non-Fermi-liquid metals, Phys. Rev. B **82**, 045121 (2010).

[40] G. Magnifico, D. Vodola, E. Ercolessi, S. P. Kumar, M. Müller, and A. Bermudez, $\mathbb{Z}_N$ gauge theories coupled to topological fermions: QED_2 with a quantum mechanical θ angle, Phys. Rev. B **100**, 115152 (2019).

[41] Jens Nyhegn, Chia-Min Chung, and Michele Burrello, $\mathbb{Z}_N$ lattice gauge theory in a ladder geometry, Phys. Rev. Res. **3**, 013133 (2021).

[42] Sunny Pradhan, Andrea Maroncelli, and Elisa Ercolessi, Discrete Abelian lattice gauge theories on a ladder and their dualities with clock models, Phys. Rev. B **109**, 064410 (2024).

[43] Yichen Xu, Xiao-Chuan Wu, Mengxing Ye, Zhu-Xi Luo, Chao-Ming Jian, and Cenke Xu, Interaction-driven metal-insulator transition with charge fractionalization, Phys. Rev. X **12**, 021067 (2022).

[44] Abolhassan Vaezi, Z_3 generalization of the Kitaev's spin-1/2 model, Phys. Rev. B **90**, 075106 (2014).

[45] Maissam Barkeshli, Hong-Chen Jiang, Ronny Thomale, and Xiao-Liang Qi, Generalized Kitaev models and extrinsic non-Abelian twist defects, Phys. Rev. Lett. **114**, 026401 (2015).

[46] Joseph Maciejko, Xiao-Liang Qi, Andreas Karch, and Shou-Cheng Zhang, Models of three-dimensional fractional topological insulators, Phys. Rev. B **86**, 235128 (2012).

[47] Serge Florens and Antoine Georges, Slave-rotor mean-field theories of strongly correlated systems and the Mott transition in finite dimensions, Phys. Rev. B **70**, 035114 (2004).

[48] Piers Coleman, New approach to the mixed-valence problem, Phys. Rev. B **29**, 3035 (1984).

[49] Gabriel Kotliar and Andrei E. Ruckenstein, New functional integral approach to strongly correlated Fermi systems: The Gutzwiller approximation as a saddle point, Phys. Rev. Lett. **57**, 1362 (1986).

[50] N. Read and Subir Sachdev, Large-N expansion for frustrated quantum antiferromagnets, Phys. Rev. Lett. **66**, 1773 (1991).

[51] Rong Yu and Qimiao Si, $U(1)$ slave-spin theory and its application to Mott transition in a multiorbital model for iron pnictides, Phys. Rev. B **86**, 085104 (2012).

[52] Pietro M. Bonetti and Walter Metzner, SU(2) gauge theory of the pseudogap phase in the two-dimensional Hubbard model, Phys. Rev. B **106**, 205152 (2022).

[53] Zheng-Cheng Gu, Zhenghan Wang, and Xiao-Gang Wen, Lattice model for fermionic toric code, Phys. Rev. B **90**, 085140 (2014).

[54] Umberto Borla, Bhilahari Jeevanesan, Frank Pollmann, and Sergej Moroz, Quantum phases of two-dimensional $\mathbb{Z}_2$ gauge theory coupled to single-component fermion matter, Phys. Rev. B **105**, 075132 (2022).

[55] Patrick Emonts, Ariel Kelman, Umberto Borla, Sergej Moroz, Snir Gazit, and Erez Zohar, Finding the ground state of a lattice gauge theory with fermionic tensor networks: A $2 + 1D\mathbb{Z}_2$ demonstration, Phys. Rev. D **107**, 014505 (2023).

[56] Rahul Nandkishore, Max A. Metlitski, and T. Senthil, Orthogonal metals: The simplest non-Fermi liquids, Phys. Rev. B **86**, 045128 (2012).

[57] Yin Zhong, Yu-Feng Wang, and Hong-Gang Luo, Z_2 fractionalized Chern/topological insulators in an exactly soluble correlated model, Phys. Rev. B **88**, 045109 (2013).

[58] Martin Hohenadler and Fakher F. Assaad, Orthogonal metal in the Hubbard model with liberated slave spins, Phys. Rev. B **100**, 125133 (2019).

[59] A. Rüegg, S. D. Huber, and M. Sigrist, $\mathbb{Z}_2$-slave-spin theory for strongly correlated fermions, Phys. Rev. B **81**, 155118 (2010).

[60] Arun Paramekanti and Ashvin Vishwanath, Extending luttinger's theorem to Z_2 fractionalized phases of matter, Phys. Rev. B **70**, 245118 (2004).

[61] T. Senthil, Matthias Vojta, and Subir Sachdev, Weak magnetism and non-Fermi liquids near heavy-fermion critical points, Phys. Rev. B **69**, 035111 (2004).

[62] Mathias S Scheurer, Shubhayu Chatterjee, Wei Wu, Michel Ferrero, Antoine Georges, and Subir Sachdev, Topological order in the pseudogap metal, Proc. Natl. Acad. Sci. USA **115**, E3665 (2018).

[63] Elio J. König, Piers Coleman, and Alexei M. Tsvelik, Soluble limit and criticality of fermions in $\mathbb{Z}_2$ gauge theories, Phys. Rev. B **102**, 155143 (2020).

[64] J. M. Luttinger, Fermi surface and some simple equilibrium properties of a system of interacting fermions, Phys. Rev. **119**, 1153 (1960).

[65] Masaki Oshikawa, Topological approach to Luttinger's theorem and the Fermi surface of a Kondo lattice, Phys. Rev. Lett. **84**, 3370 (2000).
[66] Cyril Proust and Louis Taillefer, The remarkable underlying ground states of cuprate superconductors, Annu. Rev. Condens. Matter Phys. **10**, 409 (2019).
[67] Qimiao Si and Frank Steglich, Heavy fermions and quantum phase transitions, Science **329**, 1161 (2010).
[68] Z. Xiang, Y. Kasahara, T. Asaba, B. Lawson, C. Tinsman, Lu Chen, K. Sugimoto, S. Kawaguchi, Y. Sato, G. Li, S. Yao, Y. L. Chen, F. Iga, John Singleton, Y. Matsuda, and Lu Li, Quantum oscillations of electrical resistivity in an insulator, Science **362**, 65 (2018).
[69] G. Li, Z. Xiang, F. Yu, T. Asaba, B. Lawson, P. Cai, C. Tinsman, A. Berkley, S. Wolgast, Y. S. Eo, Dae-Jeong Kim, C. Kurdak, J. W. Allen, K. Sun, X. H. Chen, Y. Y. Wang, Z. Fisk, and Lu Li, Two-dimensional Fermi surfaces in Kondo insulator SmB_6, Science **346**, 1208 (2014).
[70] B. S. Tan, Y.-T. Hsu, B. Zeng, M. Ciomaga Hatnean, N. Harrison, Z. Zhu, M. Hartstein, M. Kiourlappou, A. Srivastava, M. D. Johannes, T. P. Murphy, J.-H. Park, L. Balicas, G. G. Lonzarich, G. Balakrishnan, and Suchitra E. Sebastian, Unconventional Fermi surface in an insulating state, Science **349**, 287 (2015).
[71] Peter Czajka, Tong Gao, Max Hirschberger, Paula Lampen-Kelley, Arnab Banerjee, Jiaqiang Yan, David G Mandrus, Stephen E Nagler, and NP Ong, Oscillations of the thermal conductivity in the spin-liquid state of α-$RuCl_3$, Nat. Phys. **17**, 915 (2021).
[72] Igor Dzyaloshinskii, Some consequences of the Luttinger theorem: The Luttinger surfaces in non-Fermi liquids and Mott insulators, Phys. Rev. B **68**, 085113 (2003).
[73] Michele Fabrizio, Spin-liquid insulators can be Landau's Fermi liquids, Phys. Rev. Lett. **130**, 156702 (2023).
[74] Niklas Wagner, Lorenzo Crippa, Adriano Amaricci, Philipp Hansmann, Marcel Klett, Elio König, Thomas Schäfer, Domenico Di Sante, Jennifer Cano, Andrew Millis *et al.*, Mott insulators with boundary zeros, Nat. Commun. **14**, 7531 (2023).
[75] Chandan Setty, Shouvik Sur, Lei Chen, Fang Xie, Haoyu Hu, Silke Paschen, Jennifer Cano, and Qimiao Si, Symmetry constraints and spectral crossing in a Mott insulator with Green's function zeros, arXiv:2301.13870.
[76] Andrea Blason and Michele Fabrizio, Unified role of Green's function poles and zeros in topological insulators, Phys. Rev. B **108**, 125115 (2023).
[77] Xiao-Gang Wen, Quantum orders in an exact soluble model, Phys. Rev. Lett. **90**, 016803 (2003).
[78] Stephen S Bullock and Gavin K Brennen, Qudit surface codes and gauge theory with finite cyclic groups, J. Phys. A: Math. Theor. **40**, 3481 (2007).
[79] Marc Daniel Schulz, Sébastien Dusuel, Roman Orus, Julien Vidal, and Kai Phillip Schmidt, Breakdown of a perturbed topological phase, New J. Phys. **14**, 025005 (2012).
[80] Liujun Zou and Jeongwan Haah, Spurious long-range entanglement and replica correlation length, Phys. Rev. B **94**, 075151 (2016).
[81] Jiannis K Pachos, *Introduction to Topological Quantum Computation* (Cambridge University Press, Cambridge, 2012).
[82] Haruki Watanabe, Meng Cheng, and Yohei Fuji, Ground state degeneracy on torus in a family of Z_N toric code, J. Math. Phys. **64**, 051901 (2023).
[83] Chuang Chen, Xiao Yan Xu, Yang Qi, and Zi Yang Meng, Metal to orthogonal metal transition, Chin. Phys. Lett. **37**, 047103 (2020).
[84] Eduardo Fradkin and Stephen H. Shenker, Phase diagrams of lattice gauge theories with Higgs fields, Phys. Rev. D **19**, 3682 (1979).
[85] I. S. Tupitsyn, A. Kitaev, N. V. Prokof'ev, and P. C. E. Stamp, Topological multicritical point in the phase diagram of the toric code model and three-dimensional lattice gauge Higgs model, Phys. Rev. B **82**, 085114 (2010).
[86] Y. Hasegawa, P. Lederer, T. M. Rice, and P. B. Wiegmann, Theory of electronic diamagnetism in two-dimensional lattices, Phys. Rev. Lett. **63**, 907 (1989).
[87] Christian Prosko, Shu-Ping Lee, and Joseph Maciejko, Simple $\mathbb{Z}_2$ lattice gauge theories at finite fermion density, Phys. Rev. B **96**, 205104 (2017).
[88] Mohammad Hossein Zarei, Ising order parameter and topological phase transitions: Toric code in a uniform magnetic field, Phys. Rev. B **100**, 125159 (2019).
[89] Tamaghna Hazra and Piers Coleman, Luttinger sum rules and spin fractionalization in the SU(N) Kondo lattice, Phys. Rev. Res. **3**, 033284 (2021).
[90] Snir Gazit, Fakher F. Assaad, and Subir Sachdev, Fermi surface reconstruction without symmetry breaking, Phys. Rev. X **10**, 041057 (2020).
[91] J. Knolle, D. L. Kovrizhin, J. T. Chalker, and R. Moessner, Dynamics of a two-dimensional quantum spin liquid: Signatures of emergent Majorana fermions and fluxes, Phys. Rev. Lett. **112**, 207203 (2014).
[92] Elio J. König, Piers Coleman, and Yashar Komijani, Frustrated Kondo impurity triangle: A simple model of deconfinement, Phys. Rev. B **104**, 115103 (2021).
[93] P. W. Anderson, Infrared catastrophe in Fermi gases with local scattering potentials, Phys. Rev. Lett. **18**, 1049 (1967).
[94] A. O. Gogolin, A. A. Nersesian, and A. M. Tsvelik, *Bosonization and Strongly Correlated Systems* (Cambridge University Press, Cambridge, 2004).
[95] P. Nozieres and C. T. De Dominicis, Singularities in the x-ray absorption and emission of metals. III. one-body theory exact solution, Phys. Rev. **178**, 1097 (1969).
[96] A. O. Gogolin, Effect of the van Hove singularities on the x-ray absorption and emission in metal, Zh. Eksp. Teor. Fiz., Pis'ma Red. **57**, 300 (1993) [JETP Lett. **57**, 311 (1993)].
[97] A. M. Polyakov, *Gauge Fields and Strings*, 1st ed. (Routledge, London, 1987).